12

From Neutral Currents to Weak Vector Bosons

The unification of weak and electromagnetic interactions, 1973–1987.

Fermi's theory of weak interactions survived nearly unaltered over the years. Its basic structure was slightly modified by the addition of Gamow–Teller terms and finally by the determination of the V-A form, but its essence as a four fermion interaction remained. Fermi's original insight was based on the analogy with electromagnetism; from the start it was clear that there might be vector particles transmitting the weak force the way the photon transmits the electromagnetic force. Since the weak interaction was of short range, the vector particle would have to be heavy, and since beta decay changed nuclear charge, the particle would have to carry charge. The weak (or W) boson was the object of many searches. No evidence of the W boson was found in the mass region up to 20 GeV.

The V-A theory, which was equivalent to a theory with a very heavy W, was a satisfactory description of all weak interaction data. Nevertheless, it was clear that the theory was not complete. As described in Chapter 6, it predicted cross sections at very high energies that violated unitarity, the basic principle that says that the probability for an individual process to occur must be less than or equal to unity. A consequence of unitarity is that the total cross section for a process with angular momentum J can never exceed $4\pi(2J+1)/p_{cm}^2$. However, we have seen that neutrino cross sections grow linearly with increasing center-of-mass energy. When the energy exceeds about 300 GeV, there would be a contradiction.

It might be hoped that the theory could be calculated more completely, to a higher order in the Fermi coupling constant. In a complete theory, these corrections could bring the predictions back into the allowed range. Unfortunately, the Fermi theory cannot be calculated to higher order because the results are infinite. Infinities arise in calculating quantum electrodynamics (QED) to higher order, as well. In QED, it is possible to absorb these infinities so that none appears in the physical results. This is impossible in the Fermi theory. Writing the Fermi theory in terms of the W bosons enhances the similarity with QED, but the infinities remain.

The first step in the solution to this problem came from C. N. Yang and R. Mills, who in 1954 developed a theory of massless interacting vector particles. This theory could accommodate particles like the photon, W^+, and W^- that would interact with one another, but it required them to be massless. The infinities in the model could be reabsorbed (the model

Downloaded from https://www.cambridge.org/core. UNIVERSIDAD AUTONOMA METROPOLITANA, on 11 Nov 2026 at 18:15:33, subject to the Cambridge Core terms of use, available at https://www.cambridge.org/core/terms. https://doi.org/10.1017/9780511609923.014

was "renormalizable"). An important advance was made by Peter Higgs, who in 1964 showed how a theory initially containing a massless photon and two scalar particles could turn into a theory with a massive vector particle and one scalar. This "Higgs mechanism" was a key ingredient in the final model.

The Standard Model of electroweak interactions, developed largely by Glashow, Weinberg, and Salam begins with massless Yang–Mills particles. These are denoted W^+, W^-, W^0, and B (not to be confused with the B meson of the previous chapter, which plays no role here). The W's form a triplet of a new symmetry, "weak isospin," while the B is an isosinglet. The Higgs mechanism is invoked to give mass to the W bosons. At the same time, the two neutral particles, W^0 and B mix to produce two physical particles, the photon (represented by the field A) and the Z. The photon, of course, is massless. The Z acquires a mass comparable to that of the W.

The Fermi theory is equivalent to the exchange of only charged weak bosons. This allows for processes like $\nu_\mu e^- \to \mu^- \nu_e$, which may be viewed as emission of a W^+ by the initial neutrino, which turns into a muon and its absorption by the electron, which turns into an electron-neutrino. When the W is emitted or absorbed, the charges of the interacting particles are changed. The currents to which the W attaches, for example $\overline{e}\gamma_\mu(1-\gamma_5)\nu_e$, are called charged currents. The process $\nu_\mu e^- \to \nu_\mu e^-$ cannot proceed in the Fermi theory because the charged current can change ν_μ only to μ^-, not to e^-, as was shown by the two-neutrino experiment discussed in Chapter 7. The Z boson adds new interactions, ones with neutral currents. The ν_μ can emit a Z which is absorbed by the electron, thus permitting the process $\nu_\mu e^- \to \nu_\mu e^-$. No charge is transferred. The existence of weak neutral currents is a dramatic prediction of the model.

In fact, neutral-current processes had been searched for in decays like $K^+ \to \pi^+ e^- e^+$ and $K_L^0 \to \mu^+\mu^-$ (where the e^+e^- or $\mu^+\mu^-$ would be viewed as coming from a virtual Z) and found to be very rare or nonexistent. These searches had been limited invariably to strangeness-changing neutral currents, for example the current that transformed a K^+ into a π^+. The reason for this limitation was simple. In most instances where there is no change of strangeness, if a Z can be exchanged, so can a photon. Thus the effect of the Z, and hence of the neutral weak current, was always masked by a much larger electromagnetic effect. One way to avoid this was to look for scattering initiated by a neutrino that emitted a Z that subsequently interacted with a nuclear target. This process could not occur electromagnetically since the neutrino does not couple to photons. The signature of such a process was the absence of a charged lepton in the final state.

Although neutral currents were predicted in the model of Glashow, Weinberg, and Salam, the intensity of the search for them increased dramatically in the early 1970s when, through the work of G. 't Hooft and others, the theory was shown to be renormalizable. Weinberg and Salam had conjectured that the theory was renormalizable, but there was no proof initially.

The discovery of neutral-weak-current interactions was made in mid 1973 by A. Lagarrigue, P. Musset, D. H. Perkins, A. Rousset, and co-workers using the Gargamelle bubble chamber at CERN (**Ref. 12.1**). The experiment used separate neutrino and antineutrino beams. The beams were overwhelmingly muon-neutrinos, so the task was

Downloaded from https://www.cambridge.org/core. UNIVERSIDAD AUTONOMA METROPOLITANA, on 11 Nov 2026 at 18:15:33, subject to the Cambridge Core terms of use, available at https://www.cambridge.org/core/terms. https://doi.org/10.1017/9780511609923.014

to demonstrate the occurrence of events without a final-state muon. Muons could be distinguished from hadrons in the bubble chamber because it was filled with a rather dense material, freon, in which most of the produced hadrons would either interact or range out. The muons, then, were signaled by the particles exiting from the chamber without undergoing a hadronic interaction.

The background with the greatest potential to obscure the results was due to neutrino interactions occurring in the shielding before the bubble chamber. Neutrons produced in these interactions could enter the bubble chamber without leaving a track and cause an event from which, of course, no muon would emerge. The Gargamelle team was able to control this background by studying a related class of events. Some ordinary charged-current events occurring within the bubble chamber yielded neutrons that subsequently had hadronic collisions inside the bubble chamber. These events were quite analogous to the background events in which the initial neutrino interaction took place in the shielding. By studying the events in which the neutron's source was apparent, it was possible to place limits on the neutron background arising outside the chamber. In addition, the neutral-current events had another characteristic that indicated they were due to neutrinos. They were evenly distributed along the length of the bubble chamber. If they had come from neutrons there would have been more of them at the front and fewer at the back as a consequence of the depletion of the neutrons traveling through the freon. The neutrinos have such a small cross section that there is no measurable attenuation.

Not only did the experiment find convincing evidence for the neutral-current events, it measured the ratio of neutral-current to charged-current events both for neutrinos and antineutrinos. This was especially important because it provided a means of measuring the value of the neutral weak charge to which the Z boson coupled.

The electroweak theory contains three fundamental parameters aside from the masses of the particles and the mixing angles in the Kobayashi–Maskawa matrix. Once these are determined, all purely electroweak processes can be predicted. To determine the three parameters, it is necessary to measure three fundamental quantities. There is, however, a great deal of freedom in choosing these experimental quantities. It is natural to take two of them to be $\alpha_{em} \approx 1/137$ and $G_F \approx 1.166 \cdot 10^{-5}$ GeV^{-2} since these are quite well measured. The third quantity must involve some new feature introduced by the electroweak model. The strength of the neutral weak currents is such a quantity. The result is often expressed in terms of the weak mixing angle θ_W that indicates the degree of mixing of the W^0 and B bosons that generates the photon and Z:

$$A = \sin\theta_W W^0 + \cos\theta_W B; \qquad W^0 = \sin\theta_W A + \cos\theta_W Z; \tag{12.1}$$

$$Z = \cos\theta_W W^0 - \sin\theta_W B; \qquad B = \cos\theta_W A - \sin\theta_W Z. \tag{12.2}$$

The photon couples to particles according to their charges. We can represent the coupling to a fermion f by

$$\overline{f}\gamma_\mu e Q f A^\mu \tag{12.3}$$

Downloaded from https://www.cambridge.org/core. UNIVERSIDAD AUTONOMA METROPOLITANA, on 11 Nov 2026 at 18:15:33, subject to the Cambridge Core terms of use, available at https://www.cambridge.org/core/terms. https://doi.org/10.1017/9780511609923.014

Table 12.1. *The weak interaction quantum numbers of quarks and leptons in the Standard Model. The subscripts indicate left-handed and right-handed components.*

	e_L	e_R	ν_L	u_L	u_R	d_L	d_R
Q	-1	-1	0	$2/3$	$2/3$	$-1/3$	$-1/3$
T_3	$-1/2$	0	$1/2$	$1/2$	0	$-1/2$	0
$\frac{1}{2}Y$	$-1/2$	-1	$-1/2$	$1/6$	$2/3$	$1/6$	$-1/3$

or, in shorthand, eQA, where Q measures the charge of a particle in units of the proton charge, e, and A is the electromagnetic vector potential.

The absorption of a W^+ boson changes an electron into a neutrino. This action can be represented by the isospin operator T_+ if the neutrino and electron form a doublet with the neutrino being the $T_3 = 1/2$ component. Of course, we already know that it is only the left-handed component of the electron that participates, so we assign zero weak isospin to the right-handed part of the electron. The quarks are treated analogously, with the absorption of a W^+ changing a left-handed d into a left-handed u.

The B boson couples to fermions according to another new quantum number, the "weak hypercharge," Y. These new quantum numbers satisfy an analog of the Gell-Mann–Nishijima relation $Q = T_3 + Y/2$ as shown in Table 12.1.

After the mixing of the B and W^0 that produces the photon and the Z, the coupling of the photon to fermions is given by eQ and that of the Z by

$$\frac{e}{\sin\theta_W \cos\theta_W}\left[T_3 - Q\sin^2\theta_W\right] \tag{12.4}$$

where T_3 has an implicit $(1-\gamma_5)/2$ included to project out the left-hand part of the fermion. This is explained in greater detail below. Because the Z couples differently to left-handed and right-handed fermions, its interactions are parity violating. By comparing the couplings of the Z to that of the W, it is possible to derive a relation for the ratio of neutral-current events to charged-current events in deep inelastic neutrino scattering, NC/CC, using the parton model discussed in Chapter 8. Although the parton model is expected to work best at very high energies, the early Gargamelle results on charged currents showed that the model worked well even at the low energies available to Gargamelle using the CERN Proton Synchrotron. If the scattering of the neutrinos from antiquarks is ignored (a 10–20% correction), the predictions are

$$R_\nu = \left(\frac{NC}{CC}\right)_\nu = \frac{1}{2} - \sin^2\theta_W + \frac{20}{27}\sin^4\theta_W, \tag{12.5}$$

Downloaded from https://www.cambridge.org/core. UNIVERSIDAD AUTONOMA METROPOLITANA, on 11 Nov 2026 at 18:15:33, subject to the Cambridge Core terms of use, available at https://www.cambridge.org/core/terms. https://doi.org/10.1017/9780511609923.014

$$R_{\overline{\nu}} = \left(\frac{NC}{CC}\right)_{\overline{\nu}} = \frac{1}{2} - \sin^2\theta_W + \frac{20}{9}\sin^4\theta_W. \tag{12.6}$$

In these relations, it is assumed that

$$m_Z^2 = m_W^2/\cos^2\theta_W, \tag{12.7}$$

a prediction of the simplest version of the Standard Model of electroweak interactions as discussed below. The Gargamelle results indicated that $\sin^2\theta_W$ was in the range 0.3 to 0.4.

These results were followed by confirmation from other laboratories. The neutral-current events were not rare. They were easy to find. The problem was to demonstrate that they were not due to any of the various backgrounds. The Harvard–Penn–Wisconsin (HPW) experiment at Fermilab did verify the result, but only after some considerable difficulty in determining their efficiency for identifying muons (Ref. 12.2). The HPW experiment was a counter experiment. The target and detector were combined into a segmented unit. This was followed by a muon spectrometer. A diagram of the apparatus and the appearance of an event in the detector are shown in Figure 12.1. Inevitably there was the problem of determining how many muons failed, for geometrical reasons, to enter the muon spectrometer.

Another Fermilab experiment, a Caltech–Fermilab collaboration, also confirmed the existence of neutral currents (Ref. 12.3). A good measurement of $\sin^2\theta_W$, however, had to await the results of the CERN experiments, carried out by the CDHS, CHARM, and BEBC collaborations mentioned in Chapter 8. The CERN experiments used a beam from the Super Proton Synchrotron (SPS). The values obtained were about 0.30 for R_ν and 0.38 for $R_{\overline{\nu}}$. Later analyses of the neutral-current data found a value $\sin^2\theta_W = 0.23$.

The existence of the neutral currents was important circumstantial evidence for the electroweak model. The neutral-current to charged-current ratios lay close to the curve required by the model. Very impressive evidence came from a different kind of neutral-current experiment performed at SLAC. This experiment measured the interference between an electromagnetic amplitude and one due to neutral weak currents.

The experiment of Prescott and co-workers (**Ref. 12.4**) measured the scattering of longitudinally polarized electrons from a deuterium target. A dependence of the cross section on the value of $\boldsymbol{\sigma}_e \cdot \mathbf{p}_e$, where $\boldsymbol{\sigma}_e$ is the electron's spin, is necessarily a parity violation since this is a pseudoscalar quantity. The experiment actually measured the asymmetry

$$A = \frac{\sigma_R - \sigma_L}{\sigma_R + \sigma_L}. \tag{12.8}$$

where the subscript on the cross section indicates a right-handed or left-handed electron incident.

The right-handed and left-handed electron beams were produced by a source using a laser shining on a GaAs crystal. A Pockels cell allowed linearly polarized laser light to be changed into circularly polarized light, with the polarization changed pulse to pulse in a

Downloaded from https://www.cambridge.org/core. UNIVERSIDAD AUTONOMA METROPOLITANA, on 11 Nov 2026 at 18:15:33, subject to the Cambridge Core terms of use, available at https://www.cambridge.org/core/terms. https://doi.org/10.1017/9780511609923.014

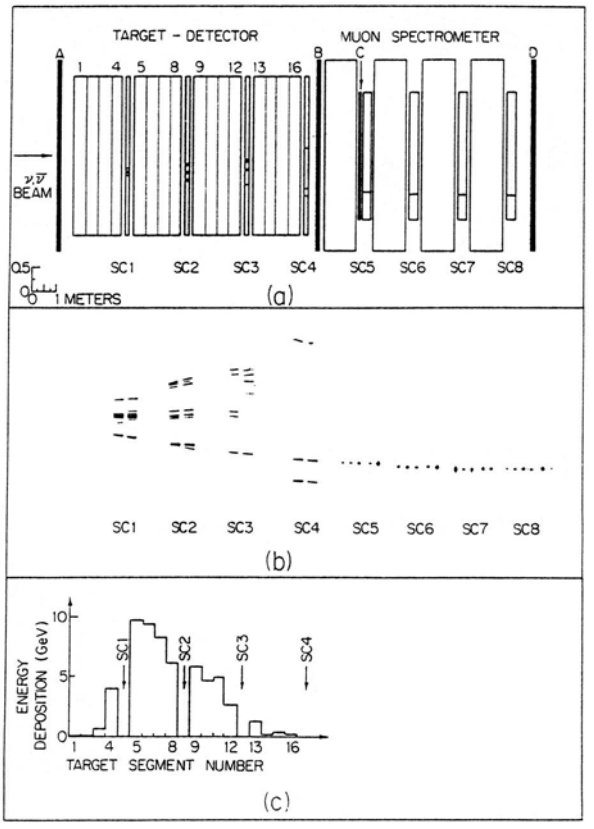


Figure 12.1. Diagram (a) of the HPW neutrino detector used at Fermilab (Ref. 12.2). There were eight spark chambers (SC) and sixteen liquid scintillator segments. The muon spectrometer contained four magnetized iron toroids. Additional scintillator counters are labeled A, B, C, D. An event is seen in the spark chambers and the same event is shown enlarged in (b). A muon track is visible in the muon spectrometer so this is a charged current event. The energy deposition for the event is displayed in (c).

random way, which was recorded. The polarized photons ejected polarized electrons from the crystal, with an average polarization of 37%.

On the basis of very general considerations, it was possible to see that the weak–electromagnetic interference effect should give A a value of order $G_F Q^2/\alpha$ where Q^2 is the momentum transferred squared of the electron (and is not to be confused with the charge operator!). A more complete calculation shows the effect ought to be about one-tenth this size, or near 10^{-4} for Q^2 of about 1 GeV^2. In order that such an effect not be masked by statistical fluctuations, about 10^{10} events are needed. This was achieved by integrating outputs of phototubes rather than counting individual events.

The scattered electrons were collected in a magnetic spectrometer like that used in the pioneering deep inelastic scattering experiments carried out 10 years before. Measurements were made for several beam energies. Because the beam was bent through an angle of 24.5°

Downloaded from https://www.cambridge.org/core. UNIVERSIDAD AUTONOMA METROPOLITANA, on 11 Nov 2026 at 18:15:33, subject to the Cambridge Core terms of use, available at https://www.cambridge.org/core/terms. https://doi.org/10.1017/9780511609923.014

before scattering, the polarized electrons precessed. This provided an additional check of the measurements.

The asymmetry can be predicted within the standard electroweak model. The result is a function of $y = (E - E')/E$, the fraction of the incident electron's energy that is lost:

$$A = \frac{-G_F Q^2}{2\sqrt{2}\pi\alpha}\frac{9}{10}\left\{1 - \frac{20}{9}\sin^2\theta_W + (1 - 4\sin^2\theta_W)\left[\frac{1-(1-y)^2}{1+(1-y)^2}\right]\right\}. \tag{12.9}$$

The result of the experiment, $A/Q^2 = (-9.5 \pm 1.6) \times 10^{-5}$ GeV^{-2}, was in good agreement with the Standard Model for a value $\sin^2\theta_W = 0.20 \pm 0.03$.

The measurement of the weak mixing angle in the neutral-current experiments made it possible to predict the masses of the W and Z. Masses arise in the Standard Model from the Higgs mechanism, which is due to hypothetical scalar particles, known as Higgs particles. The field corresponding to a neutral Higgs particle obtains a vacuum expectation value that is non-zero because this minimizes the energy of the vacuum. The various massless particles in the theory obtain masses by interacting with this ubiquitous non-zero field. The coupling of the vector (gauge) particles is governed by the analog of the usual minimal coupling of electrodynamics:

$$D_\mu = \partial_\mu - ieQA_\mu. \tag{12.10}$$

In the conventional model, the Higgs particle is part of a complex isodoublet. This is analogous to the kaon multiplet. There are four states, two charged and two neutral. We can represent this as a two component vector

$$\begin{pmatrix}\phi^+\\ \phi^0\end{pmatrix} \tag{12.11}$$

and its complex conjugate. In the vacuum, the field ϕ^0 is non-zero: $< \phi^0 >= v/\sqrt{2}$. The analog of the minimal coupling is

$$D_\mu = \partial_\mu - ig\mathbf{T}\cdot\mathbf{W}_\mu - ig'(Y/2)B_\mu \tag{12.12}$$

where the three components of $\mathbf{T}$ are the generators of the weak isospin and where g and g' are two coupling constants, one for $SU(2)$ and one for $U(1)$. Rewritten in terms of the physical particles, this is

$$D_\mu = \partial_\mu - ieQA_\mu - ig(T_+W_\mu^+ + T_-W_\mu^-)/\sqrt{2} - ig(T_3 - \sin^2\theta_W Q)Z_\mu/\cos\theta_W. \tag{12.13}$$

The relations between e, g, g', and θ_W are

$$\tan\theta_W = \frac{g'}{g}, \qquad 1/g^2 + 1/g'^2 = 1/e^2. \tag{12.14}$$

Downloaded from https://www.cambridge.org/core. UNIVERSIDAD AUTONOMA METROPOLITANA, on 11 Nov 2026 at 18:15:33, subject to the Cambridge Core terms of use, available at https://www.cambridge.org/core/terms. https://doi.org/10.1017/9780511609923.014

A comparison with the usual V-A theory shows that

$$\frac{G_F}{\sqrt{2}} = \frac{g^2}{8m_W^2}. \tag{12.15}$$

This determines the W mass:

$$m_W^2 = \frac{\pi\alpha}{\sqrt{2}\sin^2\theta_W G_F}. \tag{12.16}$$

In fact, a more precise result is obtained by using the electromagnetic coupling measured not at zero momentum transfer but rather at a momentum squared equal to m_W^2, $\alpha(m_W^2) \approx 1/129$, a value that takes into account vacuum polarization corrections. Inserting the vacuum expectation value of the Higgs field we find mass terms from

$$(D_\mu\phi)^\dagger D_\mu\phi \to \frac{1}{2}\left[\frac{g^2v^2}{4}(W_\mu^+ W^{-\mu} + W_\mu^- W^{+\mu}) + \frac{g^2v^2}{4\cos^2\theta_W} Z_\mu Z^\mu\right]. \tag{12.17}$$

This gives for the Z mass

$$m_Z^2 = m_W^2/\cos^2\theta_W \tag{12.18}$$

and with $\sin^2\theta_W = 0.23$, $m_W = 80$ GeV, $m_Z = 91$ GeV.

With a promising theory and a good measurement of $\sin^2\theta_W$, the search for the W and Z now took a different character. The masses could be predicted from the results of the neutral-current measurements of $\sin^2\theta_W$ and lay outside the range of existing machines. Following a proposal by D. Cline, C. Rubbia, and P. McIntyre, a major effort at CERN, led by C. Rubbia and S. van der Meer, transformed the SPS into a colliding beam machine, the Sp$\overline{\text{p}}$S. The regular proton beam was used to create antiprotons, which were captured and stored. The antiprotons then re-entered the SPS, but moving in the opposite direction. A particularly difficult problem was to compress the beam of antiprotons so that it would be dense enough to cause many collisions when the protons moving the other way passed through it.

If a u quark from a proton and a $\overline{d}$ quark from an antiproton collided, a W^+ could be created if the energy of the pair were near the mass of the W. The W^+ would decay into $e^+\nu$ about 8% of the time. The cross section for this process was calculated to be a fraction of a nanobarn (10^{-33}cm^2). A more spectacular signal could be obtained from Z's that decayed into e^+e^- or $\mu^+\mu^-$.

The W and Z bosons were discovered by the two large collaborations, UA-1 (**Ref. 12.5**) and UA-2 (Ref. 12.6), working at the Sp$\overline{\text{p}}$S Collider. The UA-1 detector used a uniform magnetic field of 0.7 T (7 kG) perpendicular to the beam. Inside the field was a high quality drift chamber. External to the drift chamber was extensive coverage by electromagnetic and hadronic calorimeters. The critical capability of discriminating between electrons and hadrons was achieved using many radiation lengths of material, segmented into layers.

Downloaded from https://www.cambridge.org/core. UNIVERSIDAD AUTONOMA METROPOLITANA, on 11 Nov 2026 at 18:15:33, subject to the Cambridge Core terms of use, available at https://www.cambridge.org/core/terms. https://doi.org/10.1017/9780511609923.014

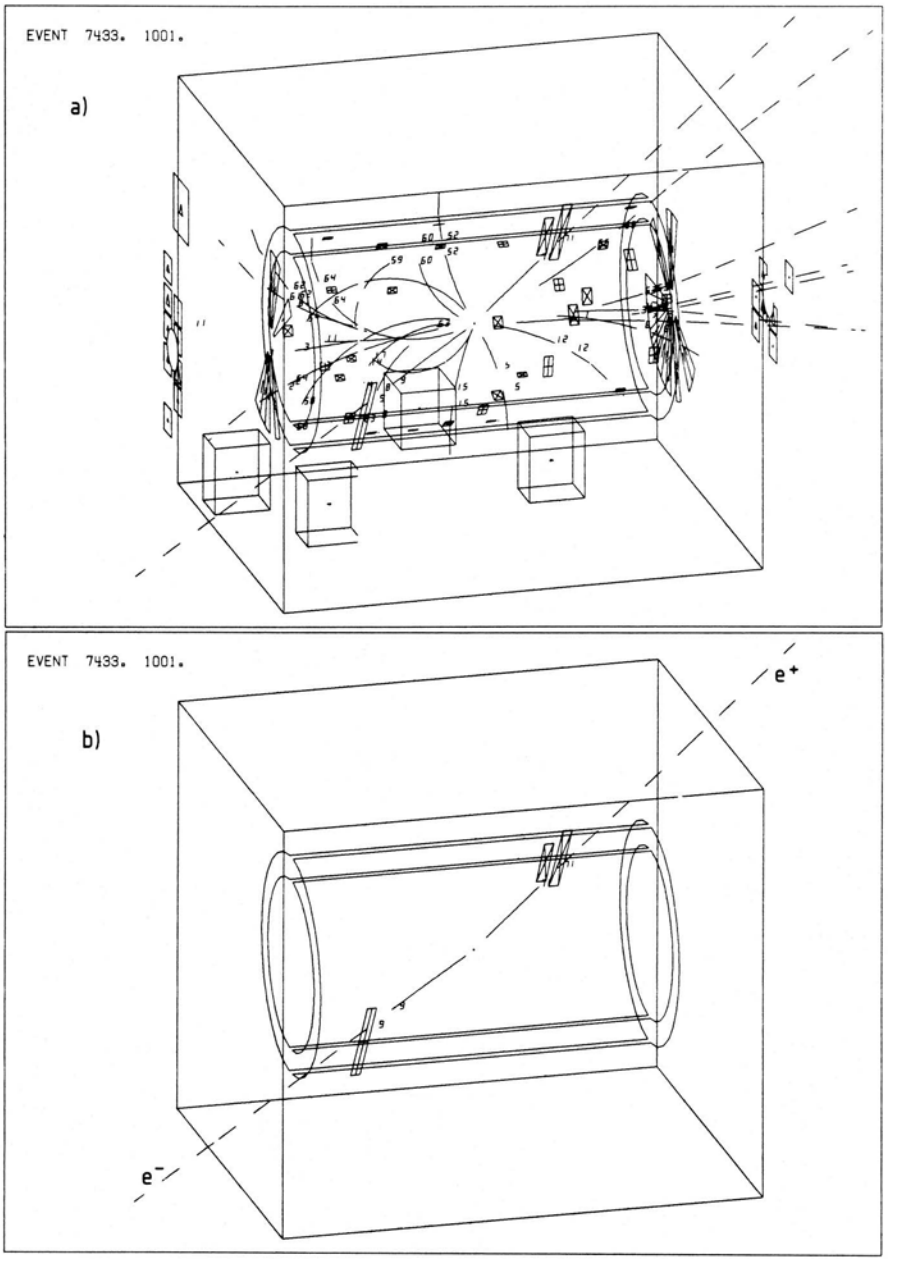


Figure 12.2. A UA-1 event display for a candidate for $Z^0 \rightarrow e^+e^-$. (a) Display of reconstructed tracks and calorimeter hits. (b) Display of tracks with $p_T > 2$ GeV/c and calorimeter hits with $E_T > 2$ GeV. The electron pair emerges cleanly from the event (Ref. 12.8).

Downloaded from https://www.cambridge.org/core. UNIVERSIDAD AUTONOMA METROPOLITANA, on 11 Nov 2026 at 18:15:33, subject to the Cambridge Core terms of use, available at https://www.cambridge.org/core/terms. https://doi.org/10.1017/9780511609923.014

By covering nearly all of the full 4π steradians with calorimetry, it was possible to check momentum balance in the plane perpendicular to the beam. This, in effect, provided a neutrino detector for those neutrinos with transverse momentum above 15 GeV or so.

In colliding-beam machines like SPEAR, DORIS, PETRA, PEP, ISR, and the Sp$\overline{\text{p}}$S Collider, the event rate is related to the cross section by

$$\text{Rate} = \mathcal{L}\sigma \tag{12.19}$$

where $\mathcal{L}$ is the luminosity and is measured in $\text{cm}^{-2}\ \text{s}^{-1}$. The luminosity depends on the density of the intersecting beams and their degree of overlap. The total number of events is $\sigma \int \mathcal{L}dt$. For the results reported by UA-1, $\int \mathcal{L}dt = 18\ \text{nb}^{-1}$ at an energy of $\sqrt{s} = 540$ GeV. The total event rate was high so various triggers were used to choose the small subset of events to be recorded.

Events with electron candidates that had high transverse momentum detected in the central part of the calorimeter and that were well-separated from any other high transverse momentum particles were selected. This class contained 39 events. Five of these contained no hadronic jets and thus had a significant transverse momentum imbalance, as would be expected for decays $W \to e\nu$. An alternative search through the same recorded events sought those with large momentum imbalance. The same five events were ultimately isolated, together with two additional events that were candidates for $W \to \tau\nu$.

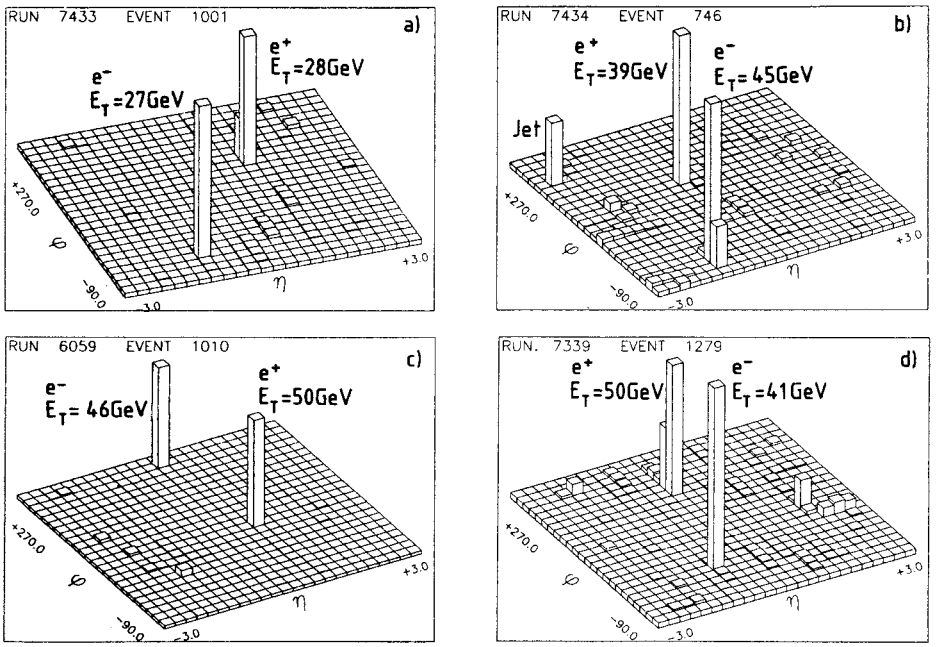


Figure 12.3. Lego plots for four UA-1 events that were candidates for $Z^0 \to e^+e^-$. The plots show the location of energy deposition in ϕ, the azimuthal angle, and $\eta = -\ln\tan(\theta/2)$, the pseudorapidity. The isolated towers of energy indicate the cleanliness of the events (Ref. 12.8).

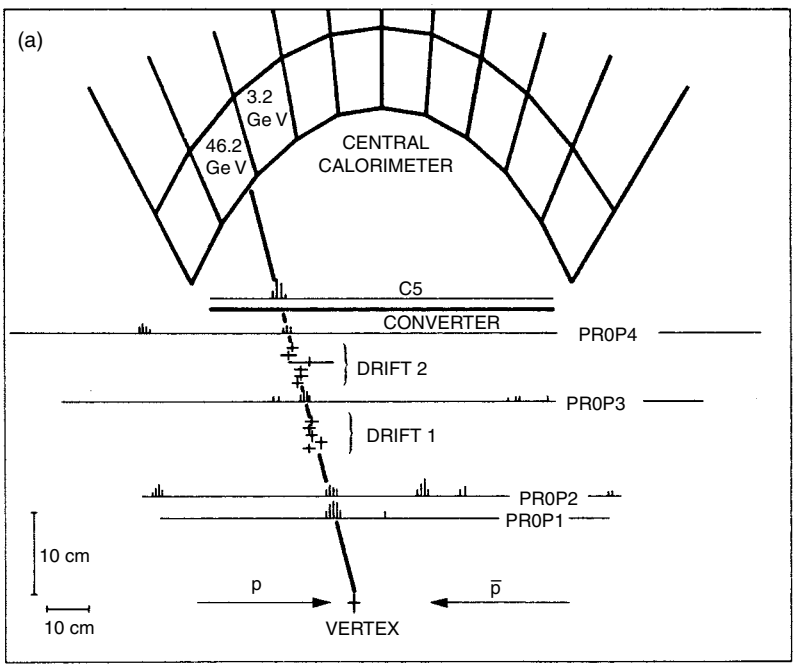
Downloaded from https://www.cambridge.org/core. UNIVERSIDAD AUTONOMA METROPOLITANA, on 11 Nov 2026 at 18:15:33, subject to the Cambridge Core terms of use, available at https://www.cambridge.org/core/terms. https://doi.org/10.1017/9780511609923.014

The mass of the W could be estimated from the observed transverse momenta. The result was $m_W = 81 \pm 5\,\text{GeV}$, in good agreement with predictions of the Standard Model using the weak mixing angle as measured in neutral-current experiments. Similar results were obtained by the UA-2 collaboration and also by observing the muonic decay of the W (Ref. 12.7).

Later, the two collaborations detected the Z through its decays $Z \to e^+e^-$ (Refs. 12.8, 12.9) and $Z \to \mu^+\mu^-$ (Ref. 12.10). This discovery took longer because the cross section for Z production is somewhat smaller than that for W's and because the branching ratios $Z \to e^+e^-$ and $Z \to \mu^+\mu^-$ are expected to be only 3% each, while $W \to e\nu$ and $W \to \mu\nu$ should be 8% each. However, the signature of two leptons with large invariant mass was unmistakable, and only a few events were necessary to establish the existence of the Z with a mass consistent with the theoretical expectation. An event that is a Z^0 candidate measured by the UA-1 Collaboration is shown in Figure 12.2. The "lego" plots for four UA-1 Z^0 candidates are shown in Figure 12.3. An event measured by the UA-2 Collaboration is shown in Figure 12.4, together with its lego plot. During running at an increased center-of-mass energy of 630 GeV additional data were accumulated. Results for the decay $Z \to e^+e^-$ obtained by the UA-1 and UA-2 Collaborations are shown in Figure 12.5.

The discovery of the W and the Z dramatically confirmed the basic features of the electroweak theory. Its unification of the seemingly unrelated phenomena of nuclear beta decay and electromagnetism is one of the major achievements of twentieth-century physics. With elegance and simplicity, it subsumes the phenomenological V-A theory, extends that theory to include neutral current phenomena and meets the theoretical demand of renormalizability. The unification of electromagnetism and weak interactions remarkably confirms Fermi's prescient observation that the fundamental process of beta decay, $n \to pe\nu$ might be viewed as the interactions of two currents. While the Fermi theory worked only in lowest order, the new theory predicted higher order radiative corrections. Just as the Lamb shift and $g - 2$ provided crucial test of QED, the real test of the electroweak theory was still to come in higher precision measurements.

Downloaded from https://www.cambridge.org/core. UNIVERSIDAD AUTONOMA METROPOLITANA, on 11 Nov 2026 at 18:15:33, subject to the Cambridge Core terms of use, available at https://www.cambridge.org/core/terms. https://doi.org/10.1017/9780511609923.014



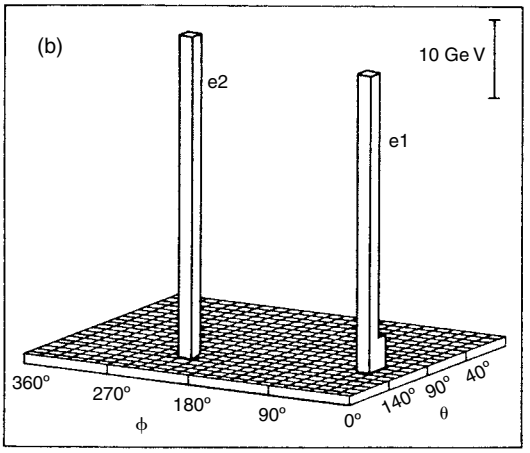


Figure 12.4. A UA-2 candidate for $Z^0 \to e^+e^-$. The upper diagram shows a track detected by a series of proportional chambers and a chamber following a tungsten converter. The calorimeter cells indicate energy measured by the electromagnetic calorimeter. The lego plot for the event shows two isolated depositions of electromagnetic energy, indicative of an e^+e^- pair (Ref. 12.9).

Downloaded from https://www.cambridge.org/core. UNIVERSIDAD AUTONOMA METROPOLITANA, on 11 Nov 2026 at 18:15:33, subject to the Cambridge Core terms of use, available at https://www.cambridge.org/core/terms. https://doi.org/10.1017/9780511609923.014

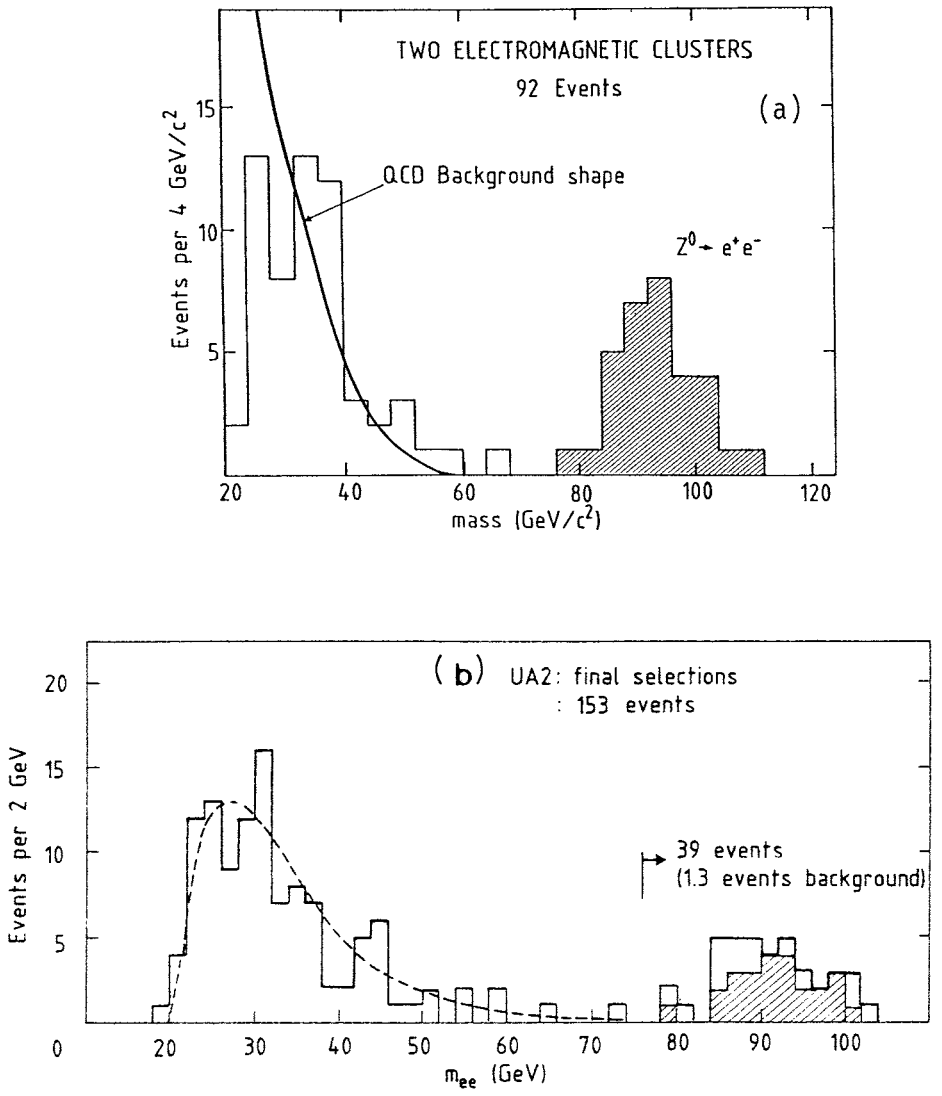


Figure 12.5. (a) The invariant mass distribution for e^+e^- pairs identified through electromagnetic calorimetry in the UA-1 detector. (Figure supplied by UA-1 Collaboration) (b) The analogous plot for the UA-2 data (Ref. 12.12). In both data sets, the Z appears well-separated from the lower mass background.

Downloaded from https://www.cambridge.org/core. UNIVERSIDAD AUTONOMA METROPOLITANA, on 11 Nov 2026 at 18:15:33, subject to the Cambridge Core terms of use, available at https://www.cambridge.org/core/terms. https://doi.org/10.1017/9780511609923.014

Exercises

12.1 Make a graph with $(NC/CC)_\nu$ as abscissa and $(NC/CC)_{\overline{\nu}}$ as ordinate. Draw the curve of values allowed by the Standard Model ignoring contributions from antiquarks. Plot the results quoted in the text. What value of $\sin^2\theta_W$ do you find?

12.2 Derive the predictions for $(NC/CC)_\nu$ and $(NC/CC)_{\overline{\nu}}$ by comparing the couplings of the W:

$$gT_+/\sqrt{2} = eT_+/\sin\theta_W\sqrt{2}$$

and the Z:

$$e(T_3 - Q\sin^2\theta_W)/\sin\theta_W\cos\theta_W.$$

Use an isoscalar target. For $|q|^2 << m_W^2, m_Z^2$, the vector boson propagator is essentially $1/m_W^2$ or $1/m_Z^2$.

12.3 Use relations analogous to those in Chapter 8 for $e_L^-\mu_L^- \rightarrow e_L^-\mu_L^-, e_R^-\mu_L^-$, etc. to derive the expression for the asymmetry, A, in polarized-electron–deuteron scattering.

12.4 The classical equation for the motion of a charged particle with mass m, charge e, and g-factor, g, in a plane perpendicular to a uniform field $\mathbf{B}$ is

$$\frac{d\boldsymbol{\beta}}{dt} = \frac{e}{m\gamma}\boldsymbol{\beta} \times \mathbf{B}$$

where $\boldsymbol{\beta}$ is the velocity vector (J. D. Jackson, *Classical Electrodynamics*, 2nd Edition, Wiley, New York, 1975. p. 559). If the direction of the spin is denoted $\mathbf{s}$, then

$$\frac{d\mathbf{s}}{dt} = \frac{e}{m}\mathbf{s} \times \left(\frac{g}{2} - 1 + \frac{1}{\gamma}\right)\mathbf{B}$$

Use these equations to verify the precession equation, Eq. (4) of Ref. 12.4.

12.5 * Assume that the W production at the Sp$\overline{\text{p}}$S Collider is due to the annihilation of a quark from the proton and an antiquark from the antiproton. Show that if the proton direction defines the z axis, the produced W's have $J_z = -1$. Show that in the W rest frame the outgoing negative leptons from $W^- \rightarrow l^-\overline{\nu}$ have the angular distribution $(1 + \cos\theta^*)^2$, while the positive leptons from $W^+ \rightarrow l^+\overline{\nu}$ have the angular distribution $(1 - \cos\theta^*)^2$, where θ^* is measured from the z (proton) direction. What is expected for Z decay? Compare with available data, *e.g.* S. Geer, in *Proceedings of the XXIII International Conference on High Energy Physics, Berkeley, 1986*, S. C. Loken ed., World Scientific, Singapore, 1987, p. 982.

Further Reading

A more theoretical, but non-technical presentation is given by C. Quigg *Gauge Theories of the Strong, Weak, and Electromagnetic Interactions*, Benjamin/Cummings, Menlo Park, CA, 1983.

Downloaded from https://www.cambridge.org/core. UNIVERSIDAD AUTONOMA METROPOLITANA, on 11 Nov 2026 at 18:15:33, subject to the Cambridge Core terms of use, available at https://www.cambridge.org/core/terms. https://doi.org/10.1017/9780511609923.014

The Standard Model is covered in E. D. Commins and P. H. Bucksbaum, *Weak Interactions of Leptons and Quarks*, Cambridge University Press, Cambridge, 1983.

A semi-popular account of the W and Z discoveries is given by P. Watkins, *Story of the W and Z*, Cambridge University Press, New York, 1986.

References

12.1 F. J. Hasert *et al.*, "Observation of Neutrino-like Interactions without Muon or Electron in the Gargamelle Neutrino Experiment." *Phys. Lett.*, **46B**, 138 (1973).

12.2 A. Benvenuti *et al.*, "Observation of Muonless Neutrino-Induced Inelastic Interactions." *Phys. Rev. Lett.*, **32**, 800 (1974).

12.3 B. C. Barish *et al.*, "Neutral Currents in High Energy Neutrino Collisions: An Experimental Search." *Phys. Rev. Lett.*, **34**, 538 (1975).

12.4 C. Y. Prescott *et al.*, "Parity Non-Conservation in Inelastic Electron Scattering." *Phys. Lett.*, **77B**, 347 (1978).

12.5 UA 1 Collaboration, "Experimental Observation of Isolated Large Transverse Energy Electrons with Associated Missing Energy at $\sqrt{s} = 540$ GeV." *Phys. Lett.*, **122B**, 103 (1983).

12.6 UA 2 Collaboration, "Observation of Single Isolated Electrons of High Transverse Momentum in Events with Missing Transverse Energy at the CERN $\overline{\text{p}}\text{p}$ Collider." *Phys. Lett.*, **122B**, 476 (1983).

12.7 UA 1 Collaboration, "Observation of the Muonic Decay of the Charged Intermediate Vector Boson." *Phys. Lett.*, **134B**, 469 (1984).

12.8 UA 1 Collaboration, "Experimental Observation of Lepton Pairs of Invariant Mass around 95 GeV/c^2 at the CERN SPS Collider." *Phys. Lett.*, **126B**, 398 (1983).

12.9 UA 2 Collaboration, "Evidence for $Z^0 \rightarrow e^+e^-$ at the CERN $\overline{\text{p}}$ p Collider." *Phys. Lett.*, **129B**, 130 (1983).

12.10 UA 1 Collaboration, "Observation of Muonic Z^0 Decay at the $\overline{\text{p}}\text{p}$ Collider." *Phys. Lett.*, **147B**, 241 (1984).

12.11 UA 1 Collaboration, "Recent Results on Intermediate Vector Boson Properties at the CERN Super Proton Synchrotron Collider." *Phys. Lett.*, **166B**, 484 (1986).

12.12 UA 2 Collaboration, "Measurements of the Standard Model Parameters from a Study of W and Z Bosons." *Phys. Lett.*, **186B**, 440 (1987).

Downloaded from https://www.cambridge.org/core. UNIVERSIDAD AUTONOMA METROPOLITANA, on 11 Nov 2026 at 18:15:33, subject to the Cambridge Core terms of use, available at https://www.cambridge.org/core/terms. https://doi.org/10.1017/9780511609923.014

Volume 46B, number 1 PHYSICS LETTERS 3 September 1973

OBSERVATION OF NEUTRINO-LIKE INTERACTIONS WITHOUT MUON OR ELECTRON IN THE GARGAMELLE NEUTRINO EXPERIMENT

F.J. HASERT, S. KABE, W. KRENZ, J. Von KROGH, D. LANSKE, J. MORFIN, K. SCHULTZE and H. WEERTS
III. Physikalisches Institut der Technischen Hochschule, Aachen, Germany

G.H. BERTRAND-COREMANS, J. SACTON, W. Van DONINCK and P. VILAIN*[1]
Interuniversity Institute for High Energies, U.L.B., V.U.B. Brussels, Belgium

U. CAMERINI*[2], D.C. CUNDY, R. BALDI, I. DANILCHENKO*[3], W.F. FRY*[2], D. HAIDT, S. NATALI*[4], P. MUSSET, B. OSCULATI, R. PALMER*[4], J.B.M. PATTISON, D.H. PERKINS*[6], A. PULLIA, A. ROUSSET, W. VENUS*[7] and H. WACHSMUTH
CERN, Geneva, Switzerland

V. BRISSON, B. DEGRANGE, M. HAGUENAUER, L. KLUBERG, U. NGUYEN-KHAC and P. PETIAU
Laboratoire de Physique Nucléaire des Hautes Energies, Ecole Polytechnique, Paris, France

E. BELOTTI, S. BONETTI, D. CAVALLI, C. CONTA*[8], E. FIORINI and M. ROLLIER
Istituto di Fisica dell'Università, Milano and I.N.F.N. Milano, Italy

B. AUBERT, D. BLUM, L.M. CHOUNET, P. HEUSSE, A. LAGARRIGUE, A.M. LUTZ, A. ORKIN-LECOURTOIS and J.P. VIALLE
Laboratoire de l'Accélérateur Linéaire, Orsay, France

F.W. BULLOCK, M.J. ESTEN, T.W. JONES, J. McKENZIE, A.G. MICHETTE*[9] G. MYATT* and W.G. SCOTT*[6,9]
University College, London, England

Received 25 July 1973

Events induced by neutral particles and producing hadrons, but no muon or electron, have been observed in the CERN neutrino experiment. These events behave as expected if they arise from neutral current induced processes. The rates relative to the corresponding charged current processes are evaluated.

We have searched for the neutral current (NC) and charged current (CC) reactions:

$$\text{NC } \nu_\mu/\bar{\nu}_\mu + \text{N} \to \nu_\mu/\bar{\nu}_\mu + \text{hadrons}, \quad (1)$$

$$\text{CC } \nu_\mu/\bar{\nu}_\mu + \text{N} \to \mu^-/\mu^+ + \text{hadrons} \quad (2)$$

which are distinguished respectively by the absence of any possible muon, or the presence of one, and only one, possible muon. A small contamination of $\nu_e/\bar{\nu}_e$ exists in the $\nu_\mu/\bar{\nu}_\mu$ beams giving some CC events which are easily recognised by the e^-/e^+ signature. The analysis is based on 83 000 ν pictures and 207 000 $\bar{\nu}$ pictures taken at CERN in the Gargamelle bubble chamber filled with freon of density 1.5×10^3 kg/m^3 ‡ The dimensions of this chamber are such that most

*[1] Chercheur agréé de L'Institut Interuniversitaire des Sciences Nucléaires, Belgique.
*[2] Also at Physics Department, University of Wisconsin.
*[3] Now at Serpukhov.
*[4] Now at University of Bari.
*[5] Now at Brookhaven National Laboratory.
*[6] Also at University of Oxford.
*[7] Now at Rutherford High Energy Laboratory.
*[8] On leave of absence from University and INFN-Pavia.
*[9] Supported by Science Research Council grant.

‡ A more detailed account of the analysis of this experiment appears in a paper to be submitted to Nuclear Physics.

Downloaded from https://www.cambridge.org/core. UNIVERSIDAD AUTONOMA METROPOLITANA, on 11 Nov 2026 at 18:15:33, subject to the Cambridge Core terms of use, available at https://www.cambridge.org/core/terms. https://doi.org/10.1017/9780511609923.014

hadrons are unambiguously identified by interaction or by range-momentum and ionisation. Any track which could possibly be due to a muon has consigned the event to reaction (2).

Analysis of the signal. To estimate the background of neutral hadrons coming from neutrino interactions in the shielding and simulating reaction (1), events where a visible charged current interaction produces an identified neutron star in the chamber (associated, AS, events) were also studied. To obtain a good estimate of the true neutral hadron direction from the direction of the observed total momentum a cut in visible total energy of > 1 GeV was applied to the NC and AS events, as well as to the hadronic part of the CC events.

We have observed, in a fiducial volume of 3 m^3, 102 NC, 428 CC and 15 AS in the ν run and 64 NC, 148 CC and 12 AS in the $\bar{\nu}$ run. Using these numbers without background substraction the ratios NC/CC are then 0.24 for ν and 0.42 for $\bar{\nu}$, whilst the NC/AS ratios are 6.8 and 5.3 respectively.

The spatial distributions of the NC events have been compared to those of the CC events and found to be similar. In particular, the distribution along the beam direction of NC (fig. 1) has the same shape as the CC distribution. In contrast the observed distribution of low energy neutral stars shows a typical exponential attenuation as expected for neutron background. The distributions of radial position, hadron total energy, and angle between measured hadron total momentum and beam direction are also indistinguishable for NC and CC.

Using the direction of measured total momentum of the hadrons in NC and CC events, a Bartlett method has been used to evaluate the apparent interaction mean free paths, λ_a, for NC and CC which are found to be compatible with infinity. For the NC events we find $\lambda_a > 2.6$ m at 90% CL; this corresponds to 3.5 times the neutron interaction length for high energy (> 1 GeV) inelastic collisions in freon.

Evaluation of the background. Since the outgoing neutrinos cannot be detected in reaction (1), the NC events may be simulated by neutral hadrons coming from the ν beam or elsewhere.

As a check for cosmic ray origin, the up-down asymmetries of NC events in vertical position and momenta have been measured and found to be $(3 \pm 8)\%$ and $(-8 \pm 8)\%$ respectively. In addition, a cosmic ray

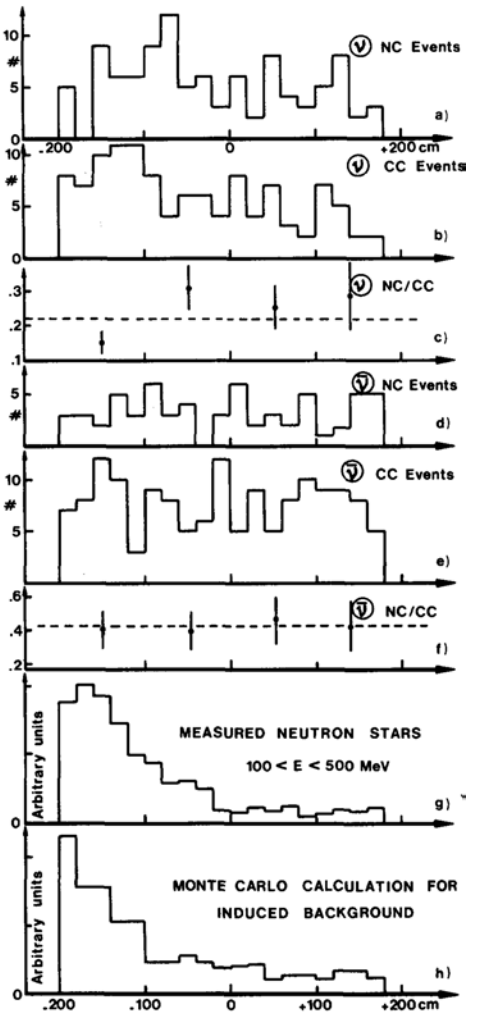


Fig. 1. Distributions along the ν-beam axis. a) NC events in ν. b) CC events in ν (this distribution is based on a reference sample of ~ 1/4 of the total ν film). c) Ratio NC/CC in ν (normalized). d) NC in $\bar{\nu}$. e) CC events in $\bar{\nu}$. f) Ratio NC/CC in $\bar{\nu}$. g) Measured neutron stars with $100 < E < 500$ MeV having protons only. h) Computed distribution of the background events from the Monte-Carlo.

Downloaded from https://www.cambridge.org/core. UNIVERSIDAD AUTONOMA METROPOLITANA, on 11 Nov 2026 at 18:15:33, subject to the Cambridge Core terms of use, available at https://www.cambridge.org/core/terms. https://doi.org/10.1017/9780511609923.014

Volume 46B, number 1 PHYSICS LETTERS 3 September 1973

exposure of 15 000 pictures shows no NC type event satisfying the selection criteria. We conclude that the cosmic background is negligible.

The low energy muons (< 100 MeV/c) captured at rest in the ν run could be mistaken as protons. A study of the observed muon spectrum in CC events, as well as a theoretical estimate of the low end of this spectrum shows that the correction to be applied is 0 ± 5 events.

Interactions of neutral hadrons produced by the primary protons up to and including the target should produce events at an equal rate in ν and $\bar{\nu}$ runs. On the contrary, we observe an absolute rate 4 times larger in the ν run than in the $\bar{\nu}$ run. If the neutral hadrons are due to defocussed secondary pions and kaons, the disagreement is larger since we expect $1-2$ times more events in $\bar{\nu}$ than in ν. Since the whole installation is shielded from below by earth we should again expect up-down asymmetries in the NC events. This is not observed.

The most important source of background is the interaction of neutral hadrons produced by the undetected neutrino interactions in the shielding. The high elasticity (0.7) of the neutrons causes a cascade effect in propagation through the shielding. The neutron energy spectrum at production can, in principle, be obtained from the AS events together with available nucleon-nucleus data. Due to the limited statistics in the AS events we make the extreme assumption that all the NC events are neutron produced an use their observed energy spectrum to calculate the neutron spectrum from neutrino interactions. This gives an energy dependence described by E^{-2}. The effective interaction length λ_e of neutrons in the shielding is then found to be 2.5 times the inelastic interaction length, λ_i. A smaller effective interaction length is found for K_L^o although the background from this source must be negligible since we find no examples of Λ^o hyperon production among the NC events.

From the absolute value of the number of AS events, we can calculate the number of background events. This has been done by Monte-Carlo generation of events in the shielding surrounding the fiducial volume according to the radial intensity distribution of the beam. The ratio of background events (B) to AS events is found to be B/AS = 0.7 for $\lambda_e = 2.5\,\lambda_i$. If the NC sample has to be explained as being entirely due to neutral hadrons, the Monte-Carlo requires $\lambda_e/\lambda_i > 10$, instead of the best estimate of 2.5. Both ratios would predict distributions along the beam direction in the chamber in strong disagreement with those observed.

Another evaluation of this type of background has been made using the simple assumption that an equilibrium of neutral hadrons with neutrinos exists throughout the entire chamber/shielding assembly. For a radially uniform ν flux it gives B/AS < 1.0 which confirms the Monte-Carlo prediction.

Conclusion. We have observed events without secondary muon or electron, induced by neutral penetrating particles. We are not able to explain the bulk of the signal by any known source of background, unless the effective interaction length of neutrons and K_L^o is at least 10 times the inelastic interaction length. These events behave similarly to the hadronic part of the charged current events. They could be attributed to neutral current induced reactions, other penetrating particles than ν_μ and ν_e, heavy leptons decaying mainly into hadrons, or by penetrating particles produced by neutrinos and in equilibrium with the ν beam.

On subtraction of the best estimate of the neutral hadron background, and taking into account the $\nu(\bar{\nu})$ contamination in the $\bar{\nu}$ (ν) beam, our best estimates of the NC/CC ratios are

$$(\mathrm{NC/CC})_\nu = 0.21 \pm 0.03$$

$$(\mathrm{NC/CC})_{\bar{\nu}} = 0.45 \pm 0.09$$

where the stated errors are statistical only. If the events are due to neutral currents, these two results are compatible with the same value of Weinberg parameter, $\sin^2\theta_W$ [1–3] in the range 0.3 to 0.4.

References

[1] S. Weinberg, Phys. Rev. D5 (1972) 1412.
[2] A. Pais and S.B. Treiman, Phys. Rev. D6 (1972) 2700.
[3] E.A. Paschos and L. Wolfenstein, Phys. Rev. D7 (1973) 91.

Downloaded from https://www.cambridge.org/core. UNIVERSIDAD AUTONOMA METROPOLITANA, on 11 Nov 2026 at 18:15:33, subject to the Cambridge Core terms of use, available at https://www.cambridge.org/core/terms. https://doi.org/10.1017/9780511609923.014

Volume 77B, number 3 PHYSICS LETTERS 14 August 1978

PARITY NON-CONSERVATION IN INELASTIC ELECTRON SCATTERING ☆

C.Y. PRESCOTT, W.B. ATWOOD, R.L.A. COTTRELL, H. DeSTAEBLER, Edward L. GARWIN, A. GONIDEC [1], R.H. MILLER, L.S. ROCHESTER, T. SATO [2], D.J. SHERDEN, C.K. SINCLAIR, S. STEIN and R.E. TAYLOR
Stanford Linear Accelerator Center, Stanford University, Stanford, CA 94305, USA

J.E. CLENDENIN, V.W. HUGHES, N. SASAO [3] and K.P. SCHÜLER
Yale University, New Haven, CT 06520, USA

M.G. BORGHINI
CERN, Geneva, Switzerland

K. LÜBELSMEYER
Technische Hochschule Aachen, Aachen, West Germany

and

W. JENTSCHKE
II. Institut für Experimentalphysik, Universität Hamburg, Hamburg, West Germany

Received 14 July 1978

We have measured parity violating asymmetries in the inelastic scattering of longitudinally polarized electrons from deuterium and hydrogen. For deuterium near $Q^2 = 1.6$ (GeV/c)^2 the asymmetry is $(-9.5 \times 10^{-5})Q^2$ with statistical and systematic uncertainties each about 10%.

We have observed a parity non-conserving asymmetry in the inelastic scattering of longitudinally polarized electrons from an unpolarized deuterium target. In this experiment a polarized electron beam of energy between 16.2 and 22.2 GeV was incident upon a liquid deuterium target. Inelastically scattered electrons from the reaction

$$e(\text{polarized}) + d \rightarrow e' + X, \qquad (1)$$

were momentum analyzed in a magnetic spectrometer at 4° and detected in a counter system instrumented to measure the electron flux, rather than to count individual scattered electrons. The momentum transfer, Q^2, to the recoiling hadronic system varied between 1 and 1.9 (GeV/c)^2 (see table 1).

Parity violating effects may arise from the interference between the weak and electromagnetic amplitudes. Calculations of the expected effects in deep inelastic experiments have been reported by several authors [1–7], and asymmetries at the level of $10^{-4}\,Q^2$ are predicted for the kinematics of our experiment. Previous experiments with muons [8] and electrons [9,10] have not achieved sufficient accuracy to observe such small effects. This same interference of amplitudes may also give rise to measurable effects in

☆ Work supported by the Dept. of Energy.

[1] Permanent address: Annecy (LAPP), 74019 Annecy-le-Vieux, France.

[2] Permanent address: National Laboratory for High Energy Physics, Tsukuba, Japan.

[3] Present address: Department of Physics, Kyoto University, Kyoto, Japan.

Downloaded from https://www.cambridge.org/core. UNIVERSIDAD AUTONOMA METROPOLITANA, on 11 Nov 2026 at 18:15:33, subject to the Cambridge Core terms of use, available at https://www.cambridge.org/core/terms. https://doi.org/10.1017/9780511609923.014

Volume 77B, number 3 PHYSICS LETTERS 14 August 1978

Table 1
Kinematic conditions at which data were taken. The average Q^2 and y values were calculated for the shower counter using a Monte Carlo program.

Beam energy E_0 (GeV)	$g-2$ precession angle θ_{prec} (rad)	Spectrometer setting E' (GeV)	Kinematic quantities averaged over spectrometer	
			Q^2 (GeV/c)^2	y
16.18	5.0π	12.5	1.05	0.18
17.80	5.5π	13.5	1.25	0.19
19.42	6.0π	14.5	1.46	0.21
22.20	6.9π	17.0	1.91	0.21

atomic spectra; experiments on transitions in the spectrum of bismuth have already been reported [11–13].

Of crucial importance to this experiment was the development of an intense source of longitudinally polarized electrons. The source consisted of a gallium arsenide crystal mounted in a structure similar to a regular SLAC gun with the GaAs replacing the usual thermionic cathode. The polarized electrons were produced by optical pumping with circularly polarized photons between the valence and conduction bands in the GaAs, which had been treated to assure a surface with negative electron affinity [14,15]. The light source was a dye laser operated at 710 nm and pulsed to match the linac (1.5 μs pulses at 120 pulses per second). Linearly polarized light from the laser was converted to circularly polarized light by a Pockels cell, a crystal with birefringence proportional to the applied electric field. The plane of polarization of the light incident on the Pockels cell could be varied by rotating a calcite prism. Reversing the sign of the high voltage pulse driving the Pockels cell reversed the helicity of the photons which in turn reversed the helicity of the electrons. This reversal was done randomly on a pulse to pulse basis. The rapid reversals minimized the effects of drifts in the experiment, and the randomization avoided changing the helicity synchronously with periodic changes in experimental parameters. Pulsed beam currents of several hundred milliamperes were achieved, with intensity fluctuations of a few percent.

The longitudinally polarized electrons were accelerated with negligible depolarization as confirmed by earlier tests [16] [‡1]. Both the sign and the magnitude of the polarization of the beam at the target were measured periodically by observing the asymmetry in Møller (elastic electron–electron) scattering from a magnetized iron foil [16]. The polarization, $|P_e|$, averaged 0.37. Each measurement had a statistical error less than 0.01; we estimate an overall systematic uncertainty of 0.02. The beam intensity at the target varied between 1 and 4×10^{11} electrons per pulse.

A schematic of the apparatus is shown in fig. 1. The target was a 30 cm cell of liquid deuterium. The spectrometer consisted of a dipole magnet, followed by a single quadrupole and a second dipole. The scattering angle was 4° and the momentum setting was about 20% below the beam energy (see table 1 for the kinematic settings). The acceptance was ±7.4 mrad in scattering angle, ±16.6 mrad in azimuth and about ±30% in momentum, as determined from a Monte Carlo model of the spectrometer.

Two separate electron detectors intercepted electrons analyzed by the spectrometer. The first was a nitrogen-filled Cerenkov counter operated at atmospheric pressure. The second was a lead-glass shower counter with a thickness of nine radiation lengths (the TA counter). Approximately 1000 scattered electrons per pulse entered the counters.

The high rates were handled by integrating the outputs of each phototube rather than by counting individual particles. For each pulse, i, the integrated output of each phototube, N_i, was divided by the integrated beam intensity (charge), Q_i, to form the yield for that pulse, $Y_i = N_i/Q_i$. For the distributions of the Y_i we verified experimentally that the (charge weighted) means of the distributions, $\langle Y \rangle$, were independent of Q, within errors of about ±0.3%, and that the (charge weighted) standard deviations, ΔY, were consistent with the statistical fluctuations expected from the number of scattered electrons per pulse. For a run with n beam pulses the statistical uncertainty on $|Y|$ was given by $\Delta Y/\sqrt{n}$.

As a check on our procedures we measured the asymmetry for a series of runs using the unpolarized beam from the regular SLAC gun for which the asymmetry should be zero. For a given run the experimental asymmetry was given by:

$$A_{exp} = [\langle Y(+) \rangle - \langle Y(-) \rangle] / [\langle Y(+) \rangle + \langle Y(-) \rangle], \qquad (2)$$

[‡1] The present experiment used the same target as ref. [16], but used a different spectrometer and detectors.

Downloaded from https://www.cambridge.org/core. UNIVERSIDAD AUTONOMA METROPOLITANA, on 11 Nov 2026 at 18:15:33, subject to the Cambridge Core terms of use, available at https://www.cambridge.org/core/terms. https://doi.org/10.1017/9780511609923.014

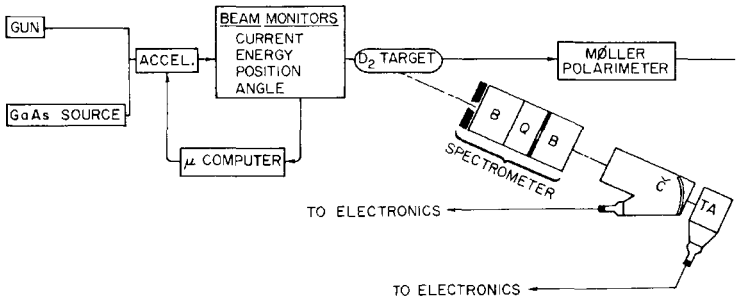


Fig. 1. Schematic layout of the experiment. Electrons from the GaAs source or the regular gun are accelerated by the linac. After momentum analysis in the beam transport system the beam passes through a liquid deuterium target. Particles scattered at 4° are analyzed in the spectrometer (bend-quad-bend) and detected in two separate counters (a gas Cerenkov counter, and a lead-glass shower counter). A beam monitoring system and a polarization analyzer are only indicated, but they provide important information in the experiment.

where + and − were assigned by the same random number generator that determined the sign of the voltage applied to the Pockels cell. For the shower counter we obtained a value of $(-2.5 \pm 2.2) \times 10^{-5}$ for A_{exp} divided by 0.37, the average value of $|P_e|$ for polarized beams from the GaAs source. The individual values were distributed about zero consistent with the calculated statistical errors. We conclude that asymmetries can be measured in this apparatus to a level of about 10^{-5}.

The same procedures were next applied to a similar series of runs using polarized beams. The helicity of the electrons coming from the source depended on the orientation of the linearly polarizing prism as well as on the sign of the voltage on the Pockels cell. Rotation of the plane of polarization by rotating the calcite prism through an angle ϕ_p caused the net electron helicity to vary as $\cos(2\phi_p)$. We chose three operating conditions:

(a) prism orientation at 0°, producing + (−) helicity electrons for + (−) Pockels cell voltage;

(b) prism orientation at 45°, producing unpolarized electrons for either sign of Pockels cell voltage; and

(c) prism orientation at 90°, producing − (+) helicity electrons for + (−) Pockels cell voltage.

Positive helicity indicates that the spin is parallel to the direction of motion. As the prism is rotated by 90°, A_{exp} should change sign since it is defined only with respect to the sign of the voltage on the Pockels cell. We may define a physics asymmetry, A, whose sign depends on the helicity of the beam at the target

$$A_{exp} = |P_e| A \cos(2\phi_p), \quad (3)$$

where ϕ_p is the angle of orientation of the calcite prism.

Fig. 2 shows the results at 19.4 GeV for $A_{exp}/|P_e|$. For the 45° point we used a value of 0.37 for $|P_e|$. These data are in satisfactory agreement with expecta-

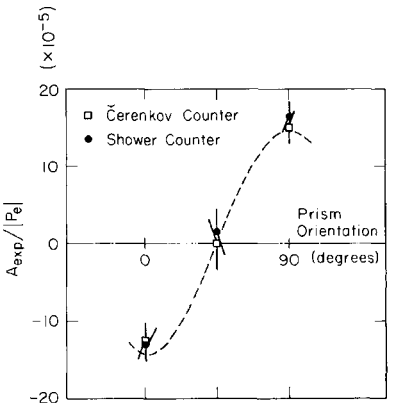


Fig. 2. The experimental asymmetry shows the expected variation (dashed line) as the beam helicity changes due to the change in orientation of the calcite prism. The data are for 19.4 GeV and deuterium. Since the same scattered particles strike both counters, they are not statistically independent. No systematic errors are shown. No corrections have been made for helicity dependent differences in beam parameters.

Downloaded from https://www.cambridge.org/core. UNIVERSIDAD AUTONOMA METROPOLITANA, on 11 Nov 2026 at 18:15:33, subject to the Cambridge Core terms of use, available at https://www.cambridge.org/core/terms. https://doi.org/10.1017/9780511609923.014

Volume 77B, number 3 PHYSICS LETTERS 14 August 1978

tions, and serve to separate effects due to the helicity of the beam from possible systematic effects associated with the reversal of the Pockels cell voltage. Only statistical errors are shown. The results at 45° are consistent with zero and indicate that other sources of error in A_{exp} must be small. Furthermore, the asymmetries measured at 0° and 90° are equal and opposite, within errors, as expected. Fig. 2 shows data from both the Cerenkov counter and the shower counter. Although these two separate counters were not statistically independent, they were analyzed with independent electronics and responded quite differently to potential backgrounds. The consistency between these counters serves as a check that such backgrounds are small.

At 19.4 GeV with the prism at 0° the helicity at the target was positive for positive Pockels cell voltage. However, this helicity depended on beam energy, owing to the $g-2$ precession of the spin in the transport magnets which deflected the beam through 24.5° before reaching the target. Because of the anomalous magnetic moment of the electron, the electron spin direction precessed relative to the momentum direction by an angle

$$\theta_{prec} = \frac{E_0}{m_e c^2}\frac{g-2}{2}\theta_{bend} = \frac{E_0\,(\mathrm{GeV})}{3.237}\,\pi\ \mathrm{rad}, \qquad (4)$$

where m_e is the mass and g the gyromagnetic ratio of the electron. Thus we expect

$$A_{exp} = |P_e|\,A\cos[(E_0\,(\mathrm{GeV})/3.237)\pi]\,, \qquad (5)$$

where the signs of values of A_{exp} for the prism at 90° have been reversed before combining with values for the prism at 0°. Fig. 3 shows the results for the kinematic points in table 1 as a function of beam energy. At each point Q^2 is different. Since we expect A to be proportional to Q^2, we divide A_{exp} by Q^2 [‡2]. Fig. 3 also shows the expected curve normalized to the point at 19.4 GeV. The data clearly follow the $g-2$ modulation of the helicity. At 17.8 GeV the spin is transverse; any effects from transverse components of the spin are expected to be negligible, in agreement with our data.

We conclude from figs. 2 and 3 that the observed asymmetries are due to electron helicity. Nevertheless,

[‡2] This fact is true in all models. It arises because the electromagnetic amplitude has a $1/Q^2$ dependence, giving an asymmetry proportional to Q^2.

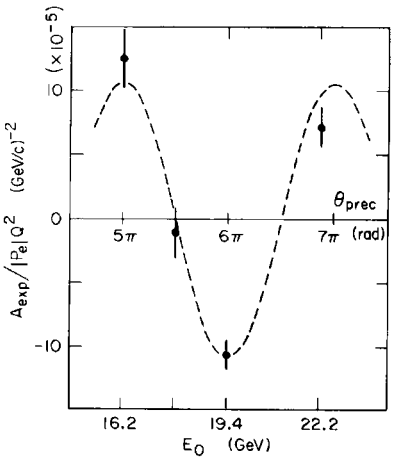


Fig. 3. The experimental asymmetry shows the expected variation (dashed line) as the beam helicity changes as a function of beam energy due to the $g-2$ precession in the beam transport system. The data are for the shower counter and the deuterium target. No systematic errors are shown. No corrections have been made for helicity dependent differences in beam parameters.

it is essential to search for and set limits on asymmetries due to effects other than helicity. Systematic effects due to slow drifts in phototube gains, magnet currents, etc., were minimized by the rapid, random reversals of polarization, and had negligible effects on A_{exp}. Effects due to random fluctuations in the beam parameters were small compared to the 3% pulse to pulse fluctuations due to counting statistics in the detectors. This was verified experimentally by measuring A_{exp} with unpolarized beams from the regular SLAC gun, and also by generating "fake" asymmetries using pulses of the same helicity from the polarized data runs themselves.

A more serious source of potential error came from small systematic differences between the beam parameters for the two helicities. Small changes in position, angle, current or energy of the beam can influence the measured yields. If these changes are correlated with reversals of the beam helicity, they may cause apparent parity violating asymmetries. Using an extensive beam monitoring system based on microwave cavities, measurements were made for each beam pulse of the average energy and position [17]. Angles were deter-

Downloaded from https://www.cambridge.org/core. UNIVERSIDAD AUTONOMA METROPOLITANA, on 11 Nov 2026 at 18:15:33, subject to the Cambridge Core terms of use, available at https://www.cambridge.org/core/terms. https://doi.org/10.1017/9780511609923.014

mined from cavities 50 m apart. The beam charge was determined using the standard toroid monitors [18]. The resolutions per pulse were about 10 μm in position, 0.3 μrad in angle, 0.01% in energy, and 0.02% in beam intensity. A microcomputer driven feedback system used position and energy signals to stabilize the average beam position, angle, and energy. Using the measured pulse to pulse beam information together with the measured sensitivities of the yield to each of the beam parameters, we made corrections to the asymmetries for helicity dependent differences in beam parameters. For these corrections, we have assigned a systematic error equal to the correction itself. The most significant imbalance was less than one part per million in E_0 which contributed -0.26×10^{-5} to A/Q^2.

We combine the values of A/Q^2 from the shower counter for the two highest energy points to obtain

$$A/Q^2 = (-9.5 \pm 1.6) \times 10^{-5}\ (\mathrm{GeV}/c)^{-2}\ \text{(deuterium)}. \quad (6)$$

We do not include the point at 16.2 GeV because it contains fairly strong elastic and resonance contributions. The sign implies a greater yield from electrons with spin antiparallel to momentum. For this combined point the average value of $y = 1 - E'/E_0$ is 0.21 and the average value of Q^2 is 1.6 $(\mathrm{GeV}/c)^2$. The quoted error, based on preliminary analysis, is derived from a statistical error of $\pm 0.86 \times 10^{-5}$ added linearly to estimated systematic uncertainties of 5% in the value of $|P_e|$, and of 3.3% from asymmetries in beam parameters. We determined experimentally that the π^- background contributed less than 0.1×10^{-5} to A/Q^2. The result in eq. (6) includes normalization corrections of 2% for the π^- background, and 3% for radiative corrections.

Any observation of non-conservation of parity in interactions involving electrons adds new information on the nature of neutral currents and gauge theories. Certain classes of gauge theory models predict no observable parity violations in experiments such as ours. Among these are those left–right symmetric models in which the difference between neutral current neutrino and anti-neutrino scattering cross sections is explained as a consequence of the handedness of the neutrino and anti-neutrino, while the underlying dynamics are parity conserving. Such models are incompatible with the results presented here.

The simplest gauge theories are based on the gauge

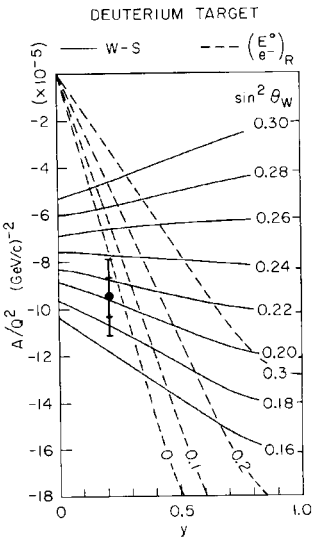


Fig. 4. Comparison of our result for deuterium with two SU(2) × U(1) predictions using the simple quark-parton model for nucleons. The outer error bars correspond to the error quoted in the text (eq. (6)). The inner error bars correspond to the statistical error. The y-dependence of A/Q^2 for various values of $\sin^2\theta_W$ is shown for two models: Weinberg–Salam (solid lines) and the hybrid model (dashed line).

group SU(2) × U(1). Within this framework the original Weinberg–Salam (W–S) model makes specific weak isospin assignments: the left-handed electron and quarks are in doublets, the right-handed electron and quarks are singlets [19]. Other assignments are possible, however. In particular, the "hybrid" or "mixed" model that assigns the right-handed electron to a doublet and the right-handed quarks to singlets has not been ruled out by neutrino experiments.

To make specific predictions for parity violation in inelastic electron scattering, it is necessary to have a model for the nucleon, and the customary one is the simple quark-parton model. The predicted asymmetries depend on the kinematic variable y as well as on the weak isospin assignments and on $\sin^2\theta_W$, where θ_W is the Weinberg angle. Fig. 4 compares our result for two SU(2) × U(1) models. The simplest model (W–S) is in good agreement with our measurement for $\sin^2\theta_W = 0.20 \pm 0.03$ which is consistent with the values obtained in neutrino experiments. The hybrid mod-

Downloaded from https://www.cambridge.org/core. UNIVERSIDAD AUTONOMA METROPOLITANA, on 11 Nov 2026 at 18:15:33, subject to the Cambridge Core terms of use, available at https://www.cambridge.org/core/terms. https://doi.org/10.1017/9780511609923.014

el is consistent with our data only for values of $\sin^2\theta_W \lesssim 0.1$.

We took a limited amount of data at 19.4 GeV using a liquid hydrogen target with the result

$$A/Q^2 = (-9.7 \pm 2.7) \times 10^{-5}\ (\mathrm{GeV}/c)^{-2}\ \text{(hydrogen)}, \quad (7)$$

where the error contains both statistical and systematic uncertainties. A proton target provides a different mix of quarks and is expected to give a slightly smaller asymmetry than deuterium [7]. Our results are not inconsistent with this expectation.

It is a pleasure to acknowledge the support we received from many people at SLAC. In particular we would like to thank M.J. Browne, G.J. Collet, R.L. Eisele, Z.D. Farkas, H.A. Hogg, C.A. Logg and H.L. Martin for especially significant contributions.

References

[1] A. Love et al., Nucl. Phys. B49 (1972) 513.
[2] E. Derman, Phys. Rev. D7 (1973) 2755.
[3] W.W. Wilson, Phys. Rev. D10 (1974) 218.
[4] S.M. Berman and J.R. Primack, Phys. Rev. D9 (1974) 2171; D10 (1974) 3895 (erratum).
[5] M.A.B. Beg and G. Feinberg, Phys. Rev. Lett. 33 (1974) 606.
[6] S.M. Bilenkii et al., Sov. J. Nucl. Phys. 21 (1975) 657.
[7] R.N. Cahn and F.J. Gilman, Phys. Rev. D17 (1978) 1313; further references to the theory may be found in this reference.
[8] Y.B. Bushnin et al., Sov. J. Nucl. Phys. 24 (1976) 279.
[9] M.J. Alguard et al., Phys. Rev. Lett. 37 (1976) 1258, 1261; 41 (1978) 70.
[10] W.B. Atwood et al., SLAC preprint SLAC-PUB-2123 (1978).
[11] L.L. Lewis et al., Phys. Rev. Lett. 39 (1977) 795.
[12] P.E.G. Baird et al., Phys. Rev. Lett. 39 (1977) 798.
[13] L.M. Barkov and M.S. Zolotorev, Zh. Eskp. Teor. Fiz. Pis'ma 26 (1978) 379.
[14] E.L. Garwin, D.T. Pierce and H.C. Siegmann, Swiss Physical Society Meeting (1974), Helv. Phys. Acta 47 (1974) 393 (abstract only); the full paper is available as SLAC-PUB-1576 (1975) (unpublished).
[15] D.T. Pierce et al., Phys. Lett. 51A (1975) 465; Appl. Phys. Lett. 26 (1975) 670.
[16] P.S. Cooper et al., Phys. Rev. Lett. 34 (1975) 1589.
[17] Z.D. Farkas et al., SLAC-PUB-1823 (1976).
[18] R.S. Larsen and D. Horelick, in: Proc. Symp. on Beam intensity measurement, DNPL/R1, Daresbury Nuclear Physics Laboratory (1968); their contribution is available as SLAC-PUB-398.
[19] S. Weinberg, Phys. Rev. Lett. 19 (1967) 1264; A. Salam, in: Elementary particle theory: relativistic groups and analyticity, Nobel Symp. No. 8, ed. N. Svartholm (Almqvist and Wiksell, Stockholm, 1968) p. 367.

Downloaded from https://www.cambridge.org/core. UNIVERSIDAD AUTONOMA METROPOLITANA, on 11 Nov 2026 at 18:15:33, subject to the Cambridge Core terms of use, available at https://www.cambridge.org/core/terms. https://doi.org/10.1017/9780511609923.014

Volume 122B, number 1 PHYSICS LETTERS 24 February 1983

EXPERIMENTAL OBSERVATION OF ISOLATED LARGE TRANSVERSE ENERGY ELECTRONS WITH ASSOCIATED MISSING ENERGY AT $\sqrt{s}$ = 540 GeV

UA1 Collaboration, CERN, Geneva, Switzerland

G. ARNISON [j], A. ASTBURY [j], B. AUBERT [b], C. BACCI [i], G. BAUER [1], A. BÉZAGUET [d], R. BÖCK [d], T.J.V. BOWCOCK [f], M. CALVETTI [d], T. CARROLL [d], P. CATZ [b], P. CENNINI [d], S. CENTRO [d], F. CERADINI [d], S. CITTOLIN [d], D. CLINE [1], C. COCHET [k], J. COLAS [b], M. CORDEN [c], D. DALLMAN [d], M. DeBEER [k], M. DELLA NEGRA [b], M. DEMOULIN [d], D. DENEGRI [k], A. Di CIACCIO [i], D. DiBITONTO [d], L. DOBRZYNSKI [g], J.D. DOWELL [c], M. EDWARDS [c], K. EGGERT [a], E. EISENHANDLER [f], N. ELLIS [d], P. ERHARD [a], H. FAISSNER [a], G. FONTAINE [g], R. FREY [h], R. FRÜHWIRTH [l], J. GARVEY [c], S. GEER [g], C. GHESQUIÈRE [g], P. GHEZ [b], K.L. GIBONI [a], W.R. GIBSON [f], Y. GIRAUD-HÉRAUD [g], A. GIVERNAUD [k], A. GONIDEC [b], G. GRAYER [j], P. GUTIERREZ [h], T. HANSL-KOZANECKA [a], W.J. HAYNES [j], L.O. HERTZBERGER [2], C. HODGES [h], D. HOFFMANN [a], H. HOFFMANN [d], D.J. HOLTHUIZEN [2], R.J. HOMER [c], A. HONMA [f], W. JANK [d], G. JORAT [d], P.I.P. KALMUS [f], V. KARIMÄKI [e], R. KEELER [f], I. KENYON [c], A. KERNAN [h], R. KINNUNEN [e], H. KOWALSKI [d], W. KOZANECKI [h], D. KRYN [d], F. LACAVA [d], J.-P. LAUGIER [k], J.-P. LEES [b], H. LEHMANN [a], K. LEUCHS [a], A. LÉVÊQUE [k], D. LINGLIN [b], E. LOCCI [k], M. LORET [k], J.-J. MALOSSE [k], T. MARKIEWICZ [d], G. MAURIN [d], T. McMAHON [c], J.-P. MENDIBURU [g], M.-N. MINARD [b], M. MORICCA [i], H. MUIRHEAD [d], F. MULLER [d], A.K. NANDI [j], L. NAUMANN [d], A. NORTON [d], A. ORKIN-LECOURTOIS [g], L. PAOLUZI [i], G. PETRUCCI [d], G. PIANO MORTARI [i], M. PIMIÄ [e], A. PLACCI [d], E. RADERMACHER [a], J. RANSDELL [h], H. REITHLER [a], J.-P. REVOL [d], J. RICH [k], M. RIJSSENBEEK [d], C. ROBERTS [j], J. ROHLF [d], P. ROSSI [d], C. RUBBIA [d], B. SADOULET [d], G. SAJOT [g], G. SALVI [f], G. SALVINI [i], J. SASS [k], J. SAUDRAIX [k], A. SAVOY-NAVARRO [k], D. SCHINZEL [f], W. SCOTT [j], T.P. SHAH [j], M. SPIRO [k], J. STRAUSS [l], K. SUMOROK [c], F. SZONCSO [l], D. SMITH [h], C. TAO [d], G. THOMPSON [f], J. TIMMER [d], E. TSCHESLOG [a], J. TUOMINIEMI [e], S. Van der MEER [d], J.-P. VIALLE [d], J. VRANA [g], V. VUILLEMIN [d], H.D. WAHL [l], P. WATKINS [c], J. WILSON [c], Y.G. XIE [d], M. YVERT [b] and E. ZURFLUH [d]

Aachen [a]–Annecy (LAPP) [b]–Birmingham [c]–CERN [d]–Helsinki [e]–Queen Mary College, London [f]–Paris (Coll. de France) [g] –Riverside [h]–Rome [i]–Rutherford Appleton Lab. [j]–Saclay (CEN) [k]–Vienna [l] Collaboration

Received 23 January 1983

We report the results of two searches made on data recorded at the CERN SPS Proton–Antiproton Collider: one for isolated large-E_T electrons, the other for large-E_T neutrinos using the technique of missing transverse energy. Both searches converge to the same events, which have the signature of a two-body decay of a particle of mass ~80 GeV/c^2. The topology as well as the number of events fits well the hypothesis that they are produced by the process $\bar{p} + p \rightarrow W^{\pm} + X$, with $W^{\pm} \rightarrow e^{\pm} + \nu$; where $W^{\pm}$ is the Intermediate Vector Boson postulated by the unified theory of weak and electromagnetic interactions.

[1] University of Wisconsin, Madison, WI, USA.
[2] NIKHEF, Amsterdam, The Netherlands.

Downloaded from https://www.cambridge.org/core. UNIVERSIDAD AUTONOMA METROPOLITANA, on 11 Nov 2026 at 18:15:33, subject to the Cambridge Core terms of use, available at https://www.cambridge.org/core/terms. https://doi.org/10.1017/9780511609923.014

Volume 122B, number 1 PHYSICS LETTERS 24 February 1983

1. Introduction. It is generally postulated that the beta decay, namely (quark) → (quark) + $e^{\pm}$ + ν is mediated by one of two charged Intermediate Vector Bosons (IVBs), W^+ and W^- of very large masses. If these particles exist, an enhancement of the cross section for the process (quark) + (antiquark) → $e^{\pm}$ + ν should occur at centre-of-mass energies in the vicinity of the IVB mass (pole), where direct experimental observation and a study of the properties of such particles become possible. The CERN Super Proton Synchrotron (SPS) Collider, in which proton and antiproton collisions at $\sqrt{s}$ = 540 GeV provide a rich sample of quark –antiquark events, has been designed with this search as the primary goal [1].

Properties of IVBs become better specified within the theoretical frame of the unified weak and electromagnetic theory and of the Weinberg–Salam model [2]. The mass of the IVB is precisely predicted [3]:

$$M_{W^{\pm}} = (82 \pm 2.4)\ \mathrm{GeV}/c^2$$

for the presently preferred [4] experimental value of the Weinberg angle $\sin^2\theta_W = 0.23 \pm 0.01$. The cross section for production is also reasonably well anticipated [5]

$$\sigma(p\bar{p} \to W^{\pm} \to e^{\pm} + \nu) \simeq 0.4 \times 10^{-33}\ k\ \mathrm{cm}^2\ ,$$

where k is an enhancement factor of ~1.5, which can be related to a similar well-known effect in the Drell–Yan production of lepton pairs. It arises from additional QCD diagrams in the production reaction with emission of gluons. In our search we have reduced the value of k by accepting only those events which show no evidence for associated jet structure in the detector.

2. The detector. The UA1 apparatus has already been extensively described elsewhere [6]. Here we concentrate on those aspects of the detector which are relevant to the present investigation.

The detector is a transverse dipole magnet which produces a uniform field of 0.7 T over a volume of 7 × 3.5 × 3.5 m^3. The interaction point is surrounded by the central detector (CD): a cylindrical drift chamber volume, 5.8 m long and 2.3 m in diameter, which yields a bubble-chamber quality picture of each $p\bar{p}$ interaction in addition to measuring momentum and specific ionization of all charged tracks.

Momentum precision for high-momentum particles is dominated by a localization error inherent to the system ($\leqslant$100 μm) and the diffusion of electrons drifting in the gas (proportional to $\sqrt{l}$ and about 350 μm after l = 22 cm maximum drift length). This results in a typical relative accuracy of ±20% for a 1 m long track at p = 40 GeV/c, and in the plane normal to the magnetic field. The precision, of course, improves considerably for longer tracks. The ionization of tracks can be measured by the classical method of the truncated mean of the 60% lowest readings to an accuracy of 10%. This allows an unambiguous identification of narrow, high-energy particle bundles (e^+e^- pairs or pencil jets) which cannot be resolved by the drift chamber digitizings.

The central section of electromagnetic and hadronic calorimetry has been used in the present investigation to identify electrons over a pseudorapidity interval $|\eta| < 3$ with full azimuthal coverage. Additional calorimetry, both electromagnetic and hadronic, extends to the forward regions of the experiment, down to 0.2° (for details, see table 1).

The central electromagnetic calorimeters consist of two different parts:

(i) 48 semicylindrical modules of alternate layers of scintillator and lead (gondolas), arranged in two cylindrical half-shells, one on either side of the beam axis with an inner radius of 1.36 m. Each module extends over approximately 180° in azimuth and measures 22.5 cm in the beam direction. The light produced in each of the four separate segmentations in depth is seen by wavelength shifter plates on each side of the counter, in turn connected to four photomultipliers (PMs), two at the top and two at the bottom. Light attenuation is exploited in order to further improve the calorimetric information: the comparison of the pulse heights of the top and bottom PM of each segment gives a measurement of the azimuthal angle ϕ for localized energy depositions, $\Delta\phi$ (rad) = 0.3/$[E(\mathrm{GeV})]^{1/2}$. A similar localization along the beam direction is possible using the complementary pairing of PMs. The energy resolution for electrons using all four PMs is $\Delta E/E = 0.15/[E(\mathrm{GeV})]^{1/2}$.

(ii) 64 petals of end-cap electromagnetic shower counters (bouchons), segmented four times in depth, on both sides of the central detector at 3 m distance from the beam crossing point. The position of each shower is measured with a position detector located inside the calorimeter at a depth of 11 radiation lengths, i.e. after the first two segments. It consists of

Downloaded from https://www.cambridge.org/core. UNIVERSIDAD AUTONOMA METROPOLITANA, on 11 Nov 2026 at 18:15:33, subject to the Cambridge Core terms of use, available at https://www.cambridge.org/core/terms. https://doi.org/10.1017/9780511609923.014

Table 1
Calorimetry.

Calorimeter	Angular coverage θ (deg)	Thickness		Cell size		Sampling step	Segmentation in depth	Resolution
		No. rad. lengths	No. abs. lengths	$\Delta\theta$ (deg)	$\Delta\phi$ (deg)			
barrel EM: gondolas	25 –155	26.4/sin θ	1.1/sin θ	5	180	1.2 mm Pb 1.5 mm scint.	3.3/6.5/10.1/6.5 X_0	$0.15/\sqrt{E}$
hadr.: c's	25 –155	–	5.0/sin θ	15	18	50 mm Fe 10 mm scint.	2.5/2.5 λ	$0.8/\sqrt{E}$
end-caps EM: bouchons	5 – 25	27/cos θ	1.1/cos θ	20	11	4 mm Pb 6 mm scint.	4/7/9/7 X_0	$0.12/\sqrt{E_T}$
hadr.: I's	155 –175	–	7.1/cos θ	5	10	50 mm Fe 10 mm scint.	3.5/3.5 λ	$0.8/\sqrt{E}$
calcom EM	0.7– 5	30	1.2	4	45	3 mm Pb 3 mm scint.	4 × 7.5 X_0	$0.15/\sqrt{E}$
hadr.	175 –179.3	–	10.2	–	–	40 mm Fe 8 mm scint.	6 × 1.7 λ	$0.8/\sqrt{E}$
very forward EM	0.2– 0.7	24.5	1.0	0.5	90	3 mm Pb 6 mm scint.	5.7/5.3/5.8/7.7 X_0	$0.15/\sqrt{E}$
hadr.	179.3–179.8	–	5.7	0.5	90	40 mm Fe 10 mm scint.	5 × 1.25 λ	$0.8/\sqrt{E}$

two planes of orthogonal proportional tubes of 2 × 2 cm^2 cross section and it locates the centre of gravity of energetic electromagnetic showers to ±2 mm in space. The attenuation length of the scintillator has been chosen to match the variation of sin θ over the radius of the calorimeters, so as to directly measure in first approximation $E_T = E \sin\theta$ rather than the true energy deposition E, which can, however, be determined later, using the information from the position detector. This technique permits us to read out directly from the end-cap detectors the amount of transverse energy deposited, without reconstruction of the event topology.

3. Electron identification. Electromagnetic showers are identified by their characteristic transition curve, and in particular by the lack of penetration in the hadron calorimeter behind them. The performance of the detectors with respect to hadrons and electrons has been studied extensively in a test beam as a function of the energy, the angle of incidence, and the location of impact. The fraction of hadrons (pions) delivering an energy deposition E_c below a given threshold in the hadron calorimeter is a rapidly falling function of energy, amounting to about 0.3% for $p \simeq 40$ GeV/c and $E_c < 200$ MeV. Under these conditions, 98% of the electrons are detected.

4. Neutrino identification. The emission of one (or more) neutrinos can be signalled only by an apparent visible energy imbalance of the event (missing energy). In order to permit such a measurement, calorimeters have been made completely hermetic down to angles of 0.2° with respect to the direction of the beams. (In practice, 97% of the mass of the magnet is calorimetrized.) It is possible to define an energy flow vector $\mathbf{\Delta E}$, adding vectorially the observed energy depositions over the whole solid angle. Neglecting particle masses and with an ideal calorimeter response and solid-angle coverage, momentum conservation requires $\mathbf{\Delta E} = 0$. We have tested this technique on minimum bias and jet-enriched events for which neutrino emission ordinarily does not occur. The transverse components ΔE_y and ΔE_z exhibit small residuals centred on zero with an rms deviation well described by the law $\Delta E_{y,z} = 0.4(\Sigma_i |E_T^i|)^{1/2}$, where all units are in GeV and the quantity under the square root is the scalar sum of all transverse energy contributions recorded in the event (fig. 1). The distributions have gaussian shape and no prominent tails. The longitudinal component

Downloaded from https://www.cambridge.org/core. UNIVERSIDAD AUTONOMA METROPOLITANA, on 11 Nov 2026 at 18:15:33, subject to the Cambridge Core terms of use, available at https://www.cambridge.org/core/terms. https://doi.org/10.1017/9780511609923.014

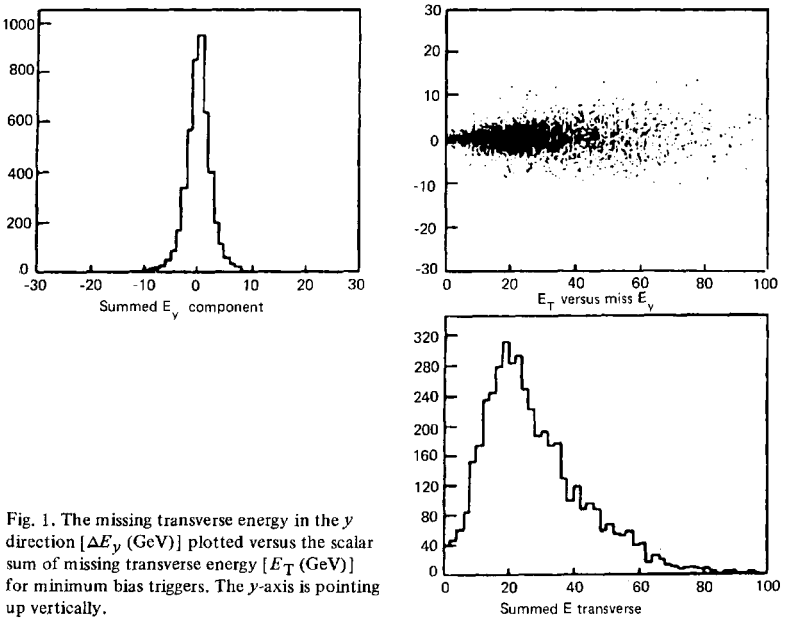


Fig. 1. The missing transverse energy in the y direction [ΔE_y (GeV)] plotted versus the scalar sum of missing transverse energy [E_T (GeV)] for minimum bias triggers. The y-axis is pointing up vertically.

of energy ΔE_x is affected by the energy flow escaping through the 0° singularity of the collider's beam pipe and it cannot be of much practical use. We remark that, like neutrinos, high-energy muons easily penetrate the calorimeter and leak out substantial amounts of energy. A muon detector, consisting of stacks of eight planes of drift chambers, surrounds the whole apparatus and has been used to identify such processes, which are occurring at the level of 1 event per nanobarn for $\Delta E_{y,z} \geqslant 10$ GeV.

5. Data-taking and initial event selections. The present work is based on data recorded in a 30-day period during November and December 1982. The integrated luminosity after subtraction of dead-time and other instrumental inefficiencies was 18 nb^{-1}, corresponding to about 10^9 collisions between protons and antiprotons at $\sqrt{s} = 540$ GeV.

For each beam–beam collision detected by scintillator hodoscopes, the energy depositions in all calorimeter cells after fast digitization were processed, in the time prior to the occurrence of the next beam–beam crossing, by a fast arithmetic processor in order to recognize the presence of a localized electromagnetic energy deposition, namely of at least 10 GeV of transverse energy either in two gondola elements or in two bouchon petals. In addition, we have simultaneously operated three other trigger conditions: (i) a jet trigger, with $\geqslant$15 GeV of transverse energy in a localized cluster [‡1] of electromagnetic and hadron calorimeters; (ii) a global E_T trigger, with >40 GeV of total transverse energy from all calorimeters with $|\eta| < 1.4$; and (iii) a muon trigger, namely at least one penetrating track with $|\eta| < 1.3$ pointing to the diamond.

The electron trigger rate was about 0.2 event per second at the (peak) luminosity $L = 5 \times 10^{28}$ cm^{-2} s^{-1}. Collisions with residual gas or with vacuum chamber walls were completely negligible, and the apparatus in normal machine conditions yielded an almost pure sample of beam–beam collisions. In total, 9.75×10^5 triggers were collected, of which 1.4×10^5 were char-

[‡1] We define a cluster as: (i) a group of eight gondolas and the two hadron calorimeter elements immediately behind; or (ii) a quadrant of bouchon elements (8) with the corresponding hadron calorimeters.

Downloaded from https://www.cambridge.org/core. UNIVERSIDAD AUTONOMA METROPOLITANA, on 11 Nov 2026 at 18:15:33, subject to the Cambridge Core terms of use, available at https://www.cambridge.org/core/terms. https://doi.org/10.1017/9780511609923.014

acterized by an electron trigger flag.

Event filtering by calorimetric information was further perfected by off-line selection of 28 000 events with $E_T > 15$ GeV in two gondolas, or $E_T > 15$ GeV in two bouchon petals with valid position-detector information. These events were finally processed with the central detector reconstruction. Of these events there are 2125 with a good quality, vertex-associated charged track of $p_T > 7$ GeV/c. This sample will be used for the subsequent analysis of events in the gondolas.

6. Search for electron candidates. We now require three conditions in succession in order to ensure that the track is isolated, namely to reject the debris of jets:

(i) The fast track ($p_T > 7$ GeV/c) as recorded by the central detector must hit a pair of adjacent gondolas with transverse energy $E_T > 15$ GeV (1106 events).

(ii) Other charged tracks, entering the same pair of gondolas, must not add up to more than 2 GeV/c of transverse momenta (276 events).

(iii) The ϕ information from pulse division from gondola phototubes must agree within 3σ with the impact of the track (167 events).

Next we introduce two simple conditions to enhance its electromagnetic nature:

(iv) The energy deposition E_c in the hadronic calorimeters aimed at by the track must not exceed 600 MeV (72 events).

(v) The energy deposited in the gondolas E_{gon} must match the measurement of the momentum of the track p_{CD}, namely $|1/p_{CD} - 1/E_{gon}| < 3\sigma$.

At this point only 39 events are left, which were individually examined by physicists on the visual scanning and interactive facility Megatek. The surviving events break up cleanly into three classes, namely 5 events with no jet activity [‡2], 11 with a jet opposite to the track within a 30° angle in ϕ, and 23 with two jets (one of which contains the electron candidate) or clear e^+e^- conversion pairs. A similar analysis performed on the bouchon has led to another event with no jets. The classes of events have striking differences. We find that whilst events with jet activity have essen-

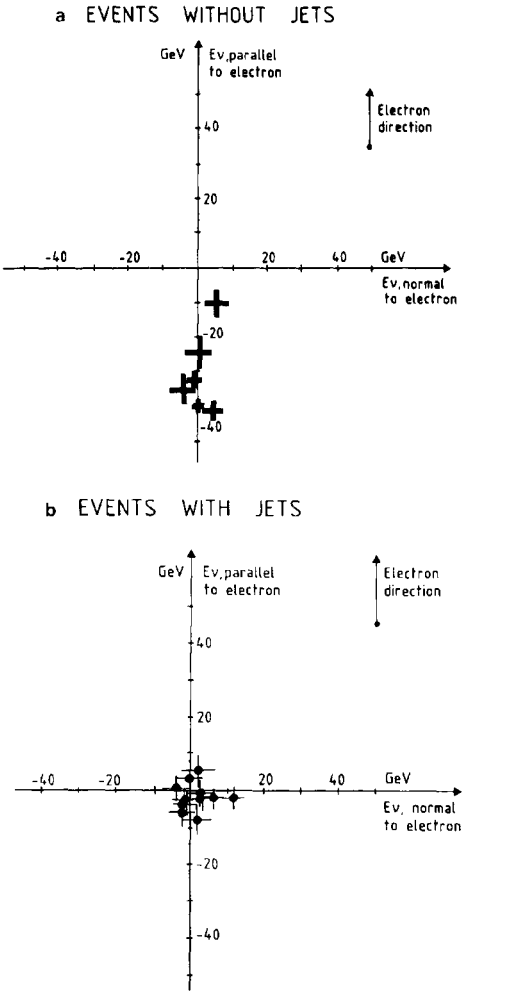


Fig. 2. The missing transverse energy (E_ν) is plotted vectorially against the electron direction for the events yielded by the electron search: (a) without jets, (b) with jets.

[‡2] The definition of a jet is based on the UA1 standard algorithm, applied separately on the calorimetry and on the central detector data. Positive results on either set are taken as evidence for a jet. In the calorimetry a four-vector (k_i, E_i) pointing to the interaction vertex is associated with each struck cell. Working in the transverse plane, all vectors with $k_T > 2.5$ GeV are ordered and are used as potential jet initiators. They are combined if their separation in phase space satisfies the cut $\Delta R = [(\Delta\eta)^2 + (\Delta\phi)^2]^{1/2} < 1$ (with ϕ in radians). The remaining soft particles are added to the nearest jet in $\Delta\eta$ and $\Delta\phi$, provided the relative p_T is < 1 GeV and $\Delta\theta < 45°$. A jet is considered valid if $E_T^{jet} > 10$ GeV. This same procedure is used for central detector tracks with appropriately adjusted parameters.

Downloaded from https://www.cambridge.org/core. UNIVERSIDAD AUTONOMA METROPOLITANA, on 11 Nov 2026 at 18:15:33, subject to the Cambridge Core terms of use, available at https://www.cambridge.org/core/terms. https://doi.org/10.1017/9780511609923.014

Volume 122B, number 1 PHYSICS LETTERS 24 February 1983

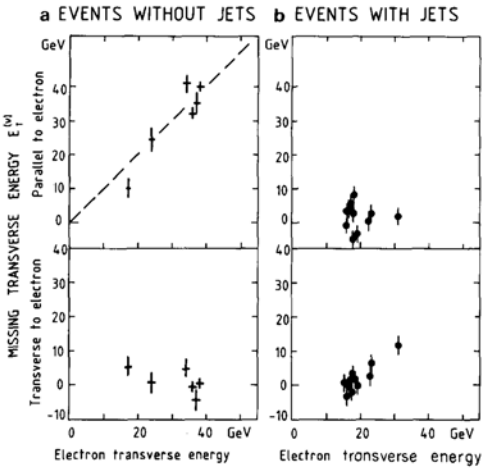


Fig. 3. The components of the missing energy parallel and perpendicular to the electron momentum plotted versus the electron energy for the events found in the electron search: (a) without jets, (b) with jets.

tially no missing energy (fig. 2b) [‡3], the ones with no jets show evidence of a missing transverse energy of the same magnitude as the transverse electron energy (fig. 3a), with the vector momenta almost exactly balanced back-to-back (fig. 2a). In order to assess how significant the effect is, we proceed to an alternative analysis based exclusively on the presence of missing transverse energy.

7. Search for events with energetic neutrinos. We start again with the initial sample of 2125 events with a charged track of $p_T > 7$ GeV/c. We now move to pick up validated events with a high missing transverse energy and with the candidate track not part of a jet:

(i) The track must point to a pair of gondolas with deposition in excess of $E_T > 15$ GeV and no other track with $p_T > 2$ GeV/c in a 20° cone (911 events).

(ii) Missing transverse energy imbalance in excess of 15 GeV.

Only 70 events survive these simple cuts, as shown in fig. 4. The previously found 5 jetless events of the gondolas are clearly visible. At this point, as for the

[‡3] The 11 events with an electron and a jet exhibit a p_T^{-4} spectrum with the highest event at $p_T = 32$ GeV/c.

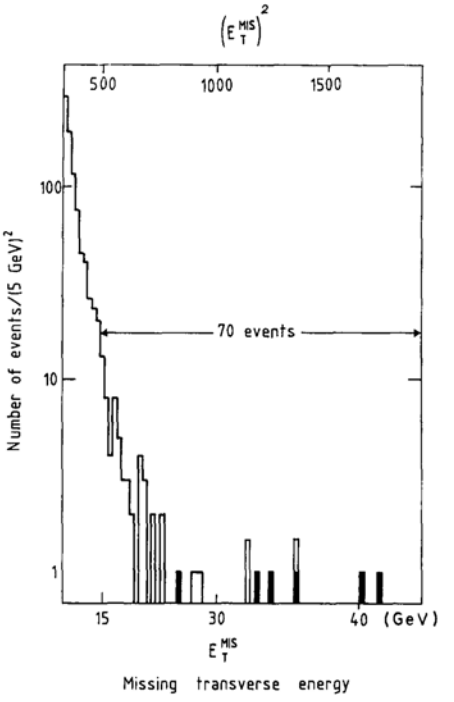


Fig. 4. The distribution of the square of the missing transverse energy for those events which survive the cuts requiring association of the central detector isolated track and a struck gondola in the missing-energy search. The five jetless events from the electron search are indicated.

electron analysis, we process the events at the interactive facility Megatek:

(iii) The missing transverse energy is validated, removing those events in which jets are pointing to where the detector response is limited, i.e. corners, light-pipe ducts going up and down. Some very evident, big secondary interactions in the beam pipe are also removed. We are left with 31 events, of which 21 have $E_c > 0.01\ E_{gon}$ and 10 events in which $E_c < 0.01\ E_{gon}$.

(iv) We require that the candidate track be well isolated, that there is no track with $p_T > 1.5$ GeV in a cone of 30°, and that $E_T < 4$ GeV for neutrals in neighbouring gondolas at similar ϕ angle. Eighteen events survive: ten with $E_c \neq 0$ and eight with $E_c = 0$.

The events once again divide naturally into the two classes: 11 events with jet activity in the azimuth op-

Downloaded from https://www.cambridge.org/core. UNIVERSIDAD AUTONOMA METROPOLITANA, on 11 Nov 2026 at 18:15:33, subject to the Cambridge Core terms of use, available at https://www.cambridge.org/core/terms. https://doi.org/10.1017/9780511609923.014

Volume 122B, number 1 PHYSICS LETTERS 24 February 1983

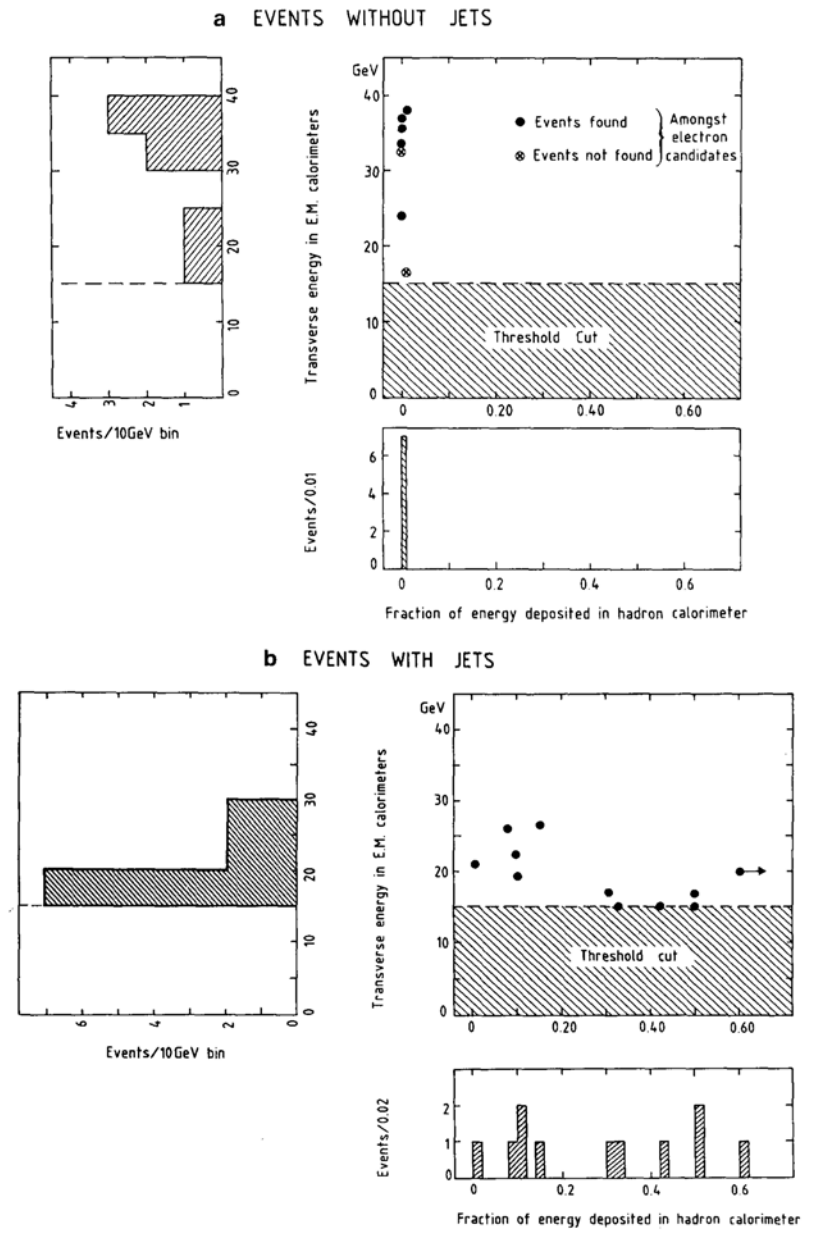


Fig. 5. A plot of the transverse energy in the EM calorimeters versus the fraction of energy deposited in the hadron calorimeters for events which survive the missing-energy search: (a) without jets, (b) with jets.

Downloaded from https://www.cambridge.org/core. UNIVERSIDAD AUTONOMA METROPOLITANA, on 11 Nov 2026 at 18:15:33, subject to the Cambridge Core terms of use, available at https://www.cambridge.org/core/terms. https://doi.org/10.1017/9780511609923.014

Table 2
Main parameters of electron events with a large missing transverse energy.

	Run, event	Properties of the electron track									Calorimeter information					General event topology				
		E_T (GeV)	E (GeV)	p (GeV/c)	Δp a)	Q	dE/dx I/I_s	y b)	Track No.	Length (m)	Sagitta (mm)	Electromagnetic energy deposition: Sample 1 (GeV)	Sample 2 (GeV)	Sample 3 (GeV)	Sample 4 (GeV)	E_{had} (GeV)	E_{tot} (GeV)	Missing E_T (GeV)	$\Delta\phi$ c) (deg.)	Charged tracks	$\sum\|E_t\|$ (GeV)
A	2958 1279	**26**	**42**	33.8	+6.3 -4.6	-	1.22 ±0.2	+1.1	36	1.36	1.7	**4**	**35**	**3**	0.2	0	278	24.4 ± 4.6	179	65	81
B	3522 214	17	46	47.5	+8.2 -6.1	-	1.37 ±0.16	+1.7	18	1.64	1.5	2	32	10	0.5	0	296	**10.9** ± 4.0	219	49	60
C	3524 197	34	45	21.6	+21.8 -7.2	-	1.37 ±0.3	-0.8	26	1.25	2.11	1	30	14	0.2	0	367	41.3 ± 3.6	187	21	68
D	3610 760	38	40	33.4	+33.0 -11.1	-	1.64 ±0.34	+0.3	9	0.98	0.75	3	9	26	2.2	0.4	111	40.0 ± 2.0	181	10	47
E	3701 305	37	37	56.2	+121.3 -22.8	+	1.54 ±0.28	-0.1	12	0.95	0.4	1	18	17	0.9	0	363	35.5 ± 4.3	173	39	87
F	4017 838	**37**	70	53.1	+6.6 -5.3	-	1.30 ±0.26	+1.4	3	2.01	2.0	19	48	3	0.3	0	177	32.3 ± 2.4	179	14	49
G	3262 1108	40	40	6.7	+1.9 -1.2	-	1.23 ±0.28	0.0	21	0.85	3.0	2	22	15	0.9	0	218	33.4 ±2.9	172	21	63

a) Including 200 μm systematic error. b) y is defined as positive in the direction of the outgoing $\bar{p}$.
c) Angle between electron and missing energy (neutrino).

Downloaded from https://www.cambridge.org/core. UNIVERSIDAD AUTONOMA METROPOLITANA, on 11 Nov 2026 at 18:15:33, subject to the Cambridge Core terms of use, available at https://www.cambridge.org/core/terms. https://doi.org/10.1017/9780511609923.014

posite to the track, and 7 events without detectable jet structure. If we now examine E_c, we see that these two classes are strikingly different, with large E_c for the events with jets (fig. 5b) and negligible E_c for the jetless ones (fig. 5a). We conclude that whilst the first ones are most likely to be hadrons, the latter constitute an electron sample.

We now compare the present result with the candidates of the previous analysis based on electron signature. We remark that five out of the seven events constitute the previous final sample (fig. 5a). Two new events have been added, eliminated previously by the test on energy matching between the central detector and the gondolas. Clearly the same physical process that provided us with the large-p_T electron delivers also high-energy neutrinos. The selectivity of our apparatus is sufficient to isolate such a process from either its electron or its neutrino features individually. If (ν_e, e) pairs and (ν_τ, τ) pairs are both produced at comparable rates, the two additional new events can readily be explained since missing energy can arise equally well from ν_e and ν_τ. Indeed, closer inspection of these events shows them to be compatible with the τ hypothesis, for instance, $\tau^- \to \pi^-\pi^0\nu_\tau$ with leading π^0. However, our isolation requirements on the charged track strongly biases against most of the τ decay modes.

8. Detailed description of the electron–neutrino events. The main properties of the final sample of six events (five gondolas, one bouchon) are given in table 2 and marked A through F. The event G is a τ candidate. One can remark that both charges of the electrons are represented. The successive energy depositions in the gondola samples are consistent with test beam findings. All but event D have no energy deposition in the hadron calorimeter; event D has a 400 MeV visible, 1% leakage beyond 26.4 radiation lengths. Test beam measurements show that this is a possible fluctuation. Multiplicity of the events is widely different: event F (fig. 6b, fig. 7b) has a small charged multiplicity (14), whilst event A (fig. 6a, fig. 7a) is very rich in particles (65). Event B is the bouchon event, and it has a number of features which must be mentioned. A 100 MeV/c track emerges from the vacuum chamber near the exit point of the electron track, which might form a part of an asymmetric electron pair with the candidate. The initial angle between the two tracks would then be 11°, not incompatible with this hypothesis once Coulomb scattering and measurement errors of the two tracks are taken into account. There is also some activity in the muon detector opposite to the electron candidate; the muon track is unmeasurable in the central detector. For these reasons we prefer to limit our final analysis to the events in the gondolas, although we believe that everything is still consistent with event B being a good event.

9. Background evaluations. We first consider possible backgrounds to the electron signature for events with no jets. Missing energy (neutrino signature) is not yet advocated. We have taken the following into consideration:

(1) A high-p_T charged pion (hadron) misidentified as an electron, or a high-p_T charged pion (hadron) overlapping with one or more π^0.

The central detector measurement obviously gives only the momentum p of the charged pion. In addition, the electromagnetic detectors can accumulate an arbitrary amount of electromagnetic energy from π^0's, which would simulate the electron behaviour. Since gondolas are thick enough to absorb the electromagnetic cascade, the energy deposition in the hadron calorimeter is dominated by the punch-through of the charged pion of momentum p measured in the central detector, for which rejection tables exist from test beam results. In our 18 nb^{-1} sample we have searched for single-track events with $p_T > 20$ GeV/c, no associated jet, $E_c > 600$ MeV to ensure hadronic signature, and a reasonable energy balance (within 3 SD) between the charged track momentum measurement and the sum of hadronic and electromagnetic energy depositions. We have found no such event. Once the measured pion rejection table is folded in, this background is entirely negligible. A further test against pile-up is given by the matching in the x-direction between the charged track of the central detector and the centroid of the energy depositions in the gondolas, and which is very good for all events.

(2) High-p_T π^0, η^0, or γ internally (Dalitz) or externally converted to an e^+e^- pair with one leg missed. The number of isolated EM conversions (π^0, η, γ, etc.) per unit of rapidity has been directly measured as a function of E_T in the bouchons, using the position detectors over the interval 10–40 GeV. From this spectrum, the Bethe–Heitler formula for pair creation, and the Kroll–Wada formula for Dalitz pairs [7], the ex-

Downloaded from https://www.cambridge.org/core. UNIVERSIDAD AUTONOMA METROPOLITANA, on 11 Nov 2026 at 18:15:33, subject to the Cambridge Core terms of use, available at https://www.cambridge.org/core/terms. https://doi.org/10.1017/9780511609923.014

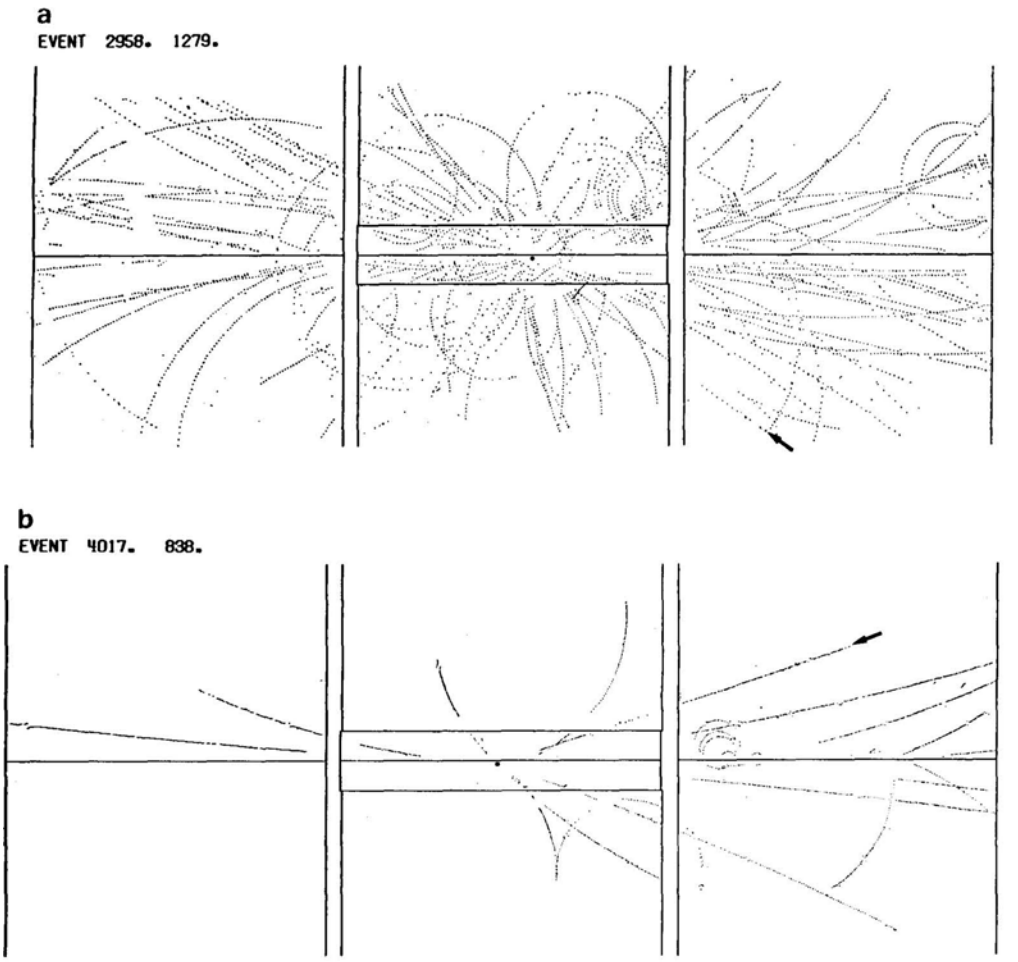


Fig. 6. The digitization from the central detector for the tracks in two of the events which have an identified, isolated, well-measured high-p_T electron: (a) high-multiplicity, 65 associated tracks; (b) low-multiplicity, 14 associated tracks.

pected number of events with a "single" $e^{\pm}$ with $p_T > 20$ GeV/c is 0.2 p_0 (GeV), largely independent of the composition of the EM component; p_0 is the effective momentum below which the low-energy leg of the pair becomes undetectable. Very conservatively, we can take $p_0 = 200$ MeV/c (curvature radius 1.2 m) and conclude that this background is negligible.

(3) Heavy quark associated production, followed by pathological fragmentation and decay configuration, such that $Q_1 \to e(\nu X)$ with the electron leading and the rest undetected, and $Q_2 \to \nu(\ell X)$, with the neutrino leading and the rest undetected. In 5 nb^{-1} we have observed one event in which there is a muon and an electron in separate jets, with $p_T^{(\mu)} = 4.4$ GeV/c and

Downloaded from https://www.cambridge.org/core. UNIVERSIDAD AUTONOMA METROPOLITANA, on 11 Nov 2026 at 18:15:33, subject to the Cambridge Core terms of use, available at https://www.cambridge.org/core/terms. https://doi.org/10.1017/9780511609923.014

Volume 122B, number 1 PHYSICS LETTERS 24 February 1983

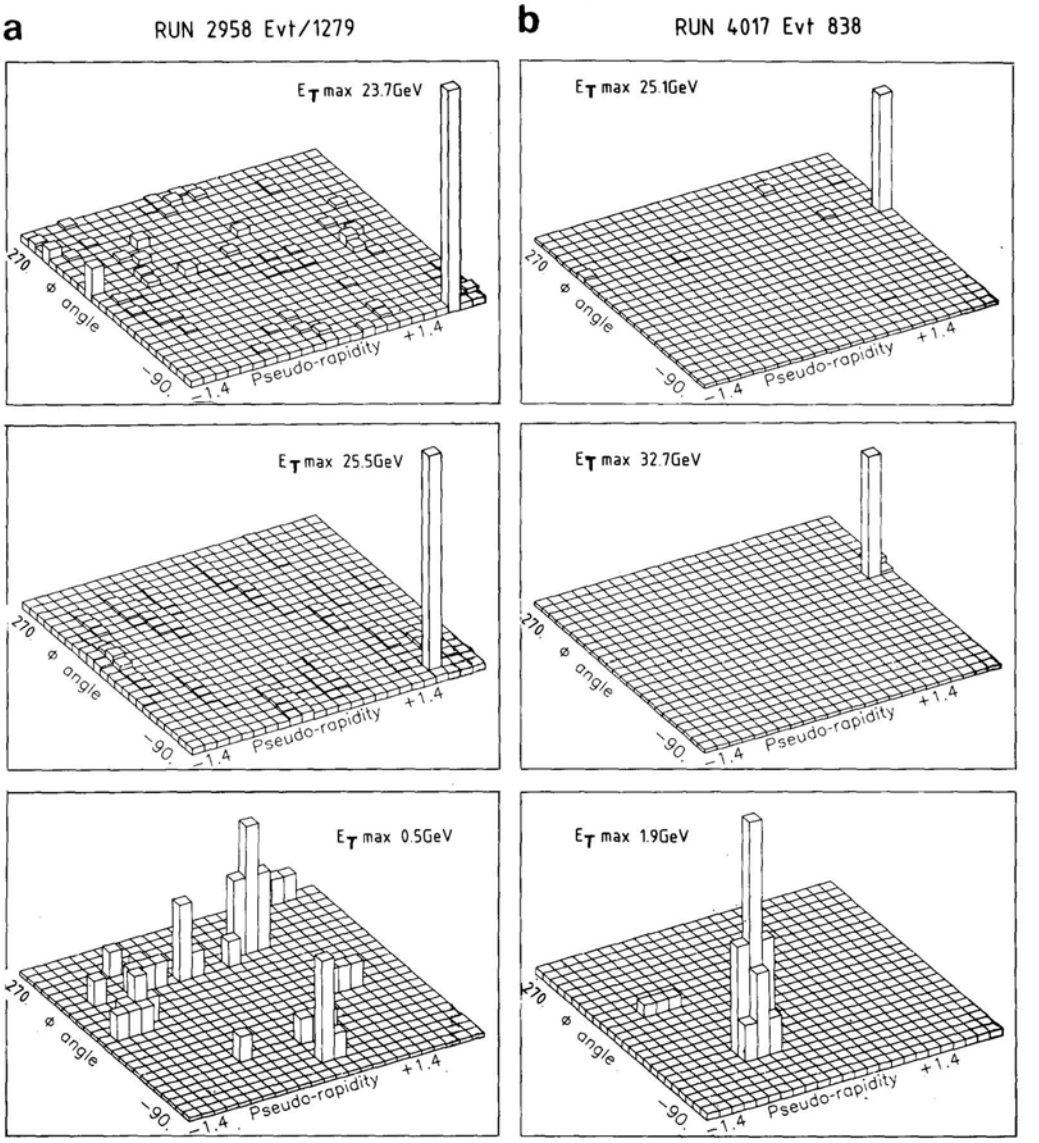


Fig. 7. The energy deposited in the cells of the central calorimetry and the equivalent plot for track momenta in the central detector for the two events of fig. 6. The top diagram shows the electromagnetic cells, the middle shows the central detector tracks, and the bottom plot, with a very much increased sensitivity, shows the energy in the hadron calorimeter. The plots reveal no hadronic energy behind the electron and no jet structure; (a) high-multiplicity; (b) low-multiplicity.

Downloaded from https://www.cambridge.org/core. UNIVERSIDAD AUTONOMA METROPOLITANA, on 11 Nov 2026 at 18:15:33, subject to the Cambridge Core terms of use, available at https://www.cambridge.org/core/terms. https://doi.org/10.1017/9780511609923.014

Volume 122B, number 1 PHYSICS LETTERS 24 February 1983

$p_T^{(e)} = 13.3$ GeV/c. Requiring (i) extrapolation to the energy of the events, (ii) fragmentation functions for leading lepton, and (iii) a detection hole for all remaining particles, makes the rate of these background events negligible.

In conclusion, we have been unable to find a background process capable of simulating the observed high-energy electrons. Thus we are led to the conclusion that they are electrons. Likewise we have searched for backgrounds capable of simulating large-E_T neutrino events. Again, none of the processes considered appear to be even near to becoming competitive.

10. Comparison between events and expectations from W decays. The simultaneous presence of an electron and (one) neutrino of approximately equal and opposite momenta in the transverse direction (fig. 8) suggests the presence of a two-body decay, $W \to e + \nu_e$. The main kinematical quantities of the events are given in table 3. A lower, model-independent bound to the W mass m_W can be obtained from the transverse mass, $m_T^2 = 2p_T^{(e)} p_T^{(\nu)} (1 - \cos\phi_{\nu e})$, remarking that $m_W \geqslant m_T$ (fig. 9). We conclude that:

$m_W > 73$ GeV/c^2 (90% confidence level).

A better accuracy can be obtained from the data if one assumes W decay kinematics and standard V – A couplings. The transverse momentum distribution of the W at production also plays a role. We can either (i) extract it from the events (table 3); or, (ii) use theoretical predictions [8].

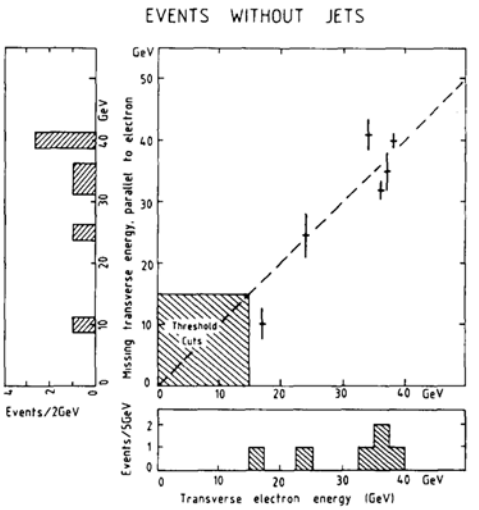


Fig. 8. The missing transverse energy component parallel to the electron, plotted versus the transverse electron energy for the final six electron events without jets (5 gondolas, 1 bouchon). All the events in the gondolas appear well above the threshold cuts used in the searches.

As one can see from fig. 10, there is good agreement between two extreme assumptions of a theoretical model [8] and our observations. By requiring no associated jet, we may have actually biased our sample towards the narrower first-order curve. Fitting of the in-

Table 3
Transverse mass and transverse momentum of a W decaying into an electron and a neutrino computed from the events of table 2.

Run, event	$p_T^{(e)}$ of electron (GeV/c)	$p_T^{(\nu)}$ = missing E_T (GeV)	Transverse mass (GeV/c)^2	$p_T^{(W)} = \lvert p_T^{(e)} + p_T^{(\nu)} \rvert$ (GeV)
A 2958 1279	24 ± 0.6	24.4 ± 4.6	48.4 ± 4.6	0.6 ± 4.6
B 3522 214	17 ± 0.4	10.9 ± 4.0	26.5 ± 4.6	10.8 ± 4.0
C 3524 197	34 ± 0.8	41.3 ± 3.6	74.8 ± 3.4	8.6 ± 3.7
D 3610 760	38 ± 1.0	40.0 ± 2.0	78.0 ± 2.2	2.1 ± 2.2
E 3701 305	37 ± 1.0	35.5 ± 4.3	72.4 ± 4.5	4.7 ± 4.4
F 4017 838	36 ± 0.7	32.3 ± 2.4	68.2 ± 2.6	3.8 ± 2.5

Downloaded from https://www.cambridge.org/core. UNIVERSIDAD AUTONOMA METROPOLITANA, on 11 Nov 2026 at 18:15:33, subject to the Cambridge Core terms of use, available at https://www.cambridge.org/core/terms. https://doi.org/10.1017/9780511609923.014

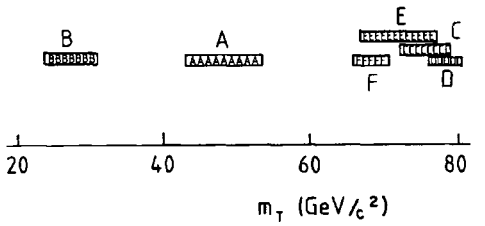


Fig. 9. The distribution of the transverse mass derived from the measured electron and neutrino vectors of the six electron events.

clusive electron spectrum and using full QCD smearing gives $m_W = (74^{+4}_{-4})$ GeV/c^2. The method finally used is the one of correcting, on an event-to-event basis, for the transverse W motion from the $(E_\nu - E_e)$ imbalance, and using the Drell–Yan predictions with no smearing. The result of a fit on electron angle and energy and neutrino transverse energy with allowance for systematic errors, is

$$m_W = (81^{+5}_{-5})\ \text{GeV}/c^2\ ,$$

in excellent agreement with the expectation of the Weinberg–Salam model [2].

We find that the number of observed events, once detection efficiencies are taken into account, is in agreement with the cross-section estimates based on structure functions, scaling violations, and the Weinberg–Salam parameters for the W particle [5].

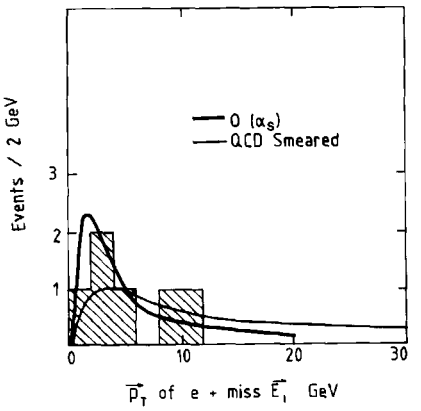


Fig. 10. The transverse momentum distribution of the W derived from our events, using the electron and missing-energy vectors. This is compared with the theoretical predictions of Halzen et al. [8] for W production without [$O(\alpha_s)$] and with QCD smearing.

We gratefully acknowledge J.B. Adams and L. Van Hove, CERN Directors-General during the initial phase of the project and without whose enthusiasm and support our work would have been impossible. The success of the collider run depended critically upon the superlative performance of the whole of the CERN accelerator complex, which was magnificently operated by its staff.

We are thankful to the management and staff of CERN and of all participating Institutes who have vigorously supported the experiment.

The following funding Agencies have contributed to this programme:

Fonds zur Förderung der Wissenschaftlichen Forschung, Austria.

Valtion luonnontieteellinen toimikunta, Finland.

Institut National de Physique Nucléaire et de Physique des Particules and Institut de Recherche Fondamentale (CEA), France.

Bundesministerium für Forschung und Technologie, Germany.

Istituto Nazionale di Fisica Nucleare, Italy.

Science and Engineering Research Council, United Kingdom.

Department of Energy, USA.

Thanks are also due to the following people who have worked with the collaboration in the preparation and data collection on the runs described here, F. Bernasconi, F. Cataneo, A.-M. Cnops, L. Dumps, J.-P. Fournier, A. Micolon, S. Palanque, P. Quéru, P. Skimming, G. Stefanini, M. Steuer, J.C. Thevenin, H. Verweij and R. Wilson.

References

[1] C. Rubbia, P. McIntyre and D. Cline, Proc. Intern. Neutrino Conf. (Aachen, 1976) (Vieweg, Braunschweig, 1977) p. 683;
Study Group, Design study of a proton–antiproton colliding beam facility, CERN/PS/AA 78-3 (1978), reprinted in Proc. Workshop on Producing high-luminosity, high-energy proton–antiproton collisions (Berkeley, 1978) report LBL-7574, UC34, p. 189;
The staff of the CERN proton–antiproton project, Phys. Lett. 107B (1981) 306.

Downloaded from https://www.cambridge.org/core. UNIVERSIDAD AUTONOMA METROPOLITANA, on 11 Nov 2026 at 18:15:33, subject to the Cambridge Core terms of use, available at https://www.cambridge.org/core/terms. https://doi.org/10.1017/9780511609923.014

[2] S. Weinberg, Phys. Rev. Lett. 19 (1967) 1264;
A. Salam, Proc. 8th Nobel Symp. (Aspenäsgården, 1968) (Almqvist and Wiksell, Stockholm, 1968) p. 367.

[3] A. Sirlin, Phys. Rev. D22 (1980) 971;
W.J. Marciano and A. Sirlin, Phys. Rev. D22 (1980) 2695;
C.H. Llewellyn Smith and J.A. Wheater, Phys. Lett. 105B (1981) 486.

[4] For a review, see: M. Davier, Proc. 21st Intern. Conf. on High-energy physics (Paris, 1982), J. Phys. (Paris) 43 (1982) C3-471.

[5] F.E. Paige, Proc. Topical Conf. on the Production of new particles at super-high energies (University of Wisconsin, Madison, 1979);
L.B. Okun and M.B. Voloshin, Nucl. Phys. B120 (1977) 459;
C. Quigg, Rev. Mod. Phys. 94 (1977) 297;
J. Kogut and J. Shigemitsu, Nucl. Phys. B129 (1977) 461;
R. Horgan and M. Jacob, Proc. CERN School of Physics (Malente, Fed. Rep. Germany, 1980), CERN 81-04, p. 65;
R.F. Peierls, T. Trueman and L.L. Wang, Phys. Rev. D16 (1977) 1397.

[6] UA1 proposal, A 4π solid-angle detector for the SPS used as a proton–antiproton collider at a centre-of-mass energy of 540 GeV, CERN/SPSC 78-06 (1978);
M. Barranco Luque et al., Nucl. Instrum. Methods 176 (1980) 175;
M. Calvetti et al., Nucl. Instrum. Methods 176 (1980) 255;
K. Eggert et al., Nucl. Instrum. Methods 176 (1980) 217, 233;
A. Astbury, Phys. Scr. 23 (1981) 397.

[7] H.M. Kroll and W. Wada, Phys. Rev. 98 (1955) 1355.

[8] F. Halzen and D.M. Scott, Phys. Lett. 78B (1978) 318;
P. Aurenche and F. Lindfors, Nucl. Phys. B185 (1981) 301;
F. Halzen, A.D. Martin, D.M. Scott and M. Dechantsreiter, Phys. Lett. 106B (1981) 147;
M. Chaichian, M. Hayashi and K. Yamagishi, Phys. Rev. D25 (1982) 130;
A. Martin, Proc. Conf. on Antiproton–proton collider physics (Madison, 1981) AIP Proc. No. 85 (American Institute of Physics, New York, 1982) p. 216;
F. Halzen, A.D. Martin and D.M. Scott, Phys. Rev. D25 (1982) 754;
V. Barger and R.J.N. Phillips, University of Wisconsin preprint MAD/PH/78 (1982).

Downloaded from https://www.cambridge.org/core. UNIVERSIDAD AUTONOMA METROPOLITANA, on 11 Nov 2026 at 18:15:33, subject to the Cambridge Core terms of use, available at https://www.cambridge.org/core/terms. https://doi.org/10.1017/9780511609923.014